



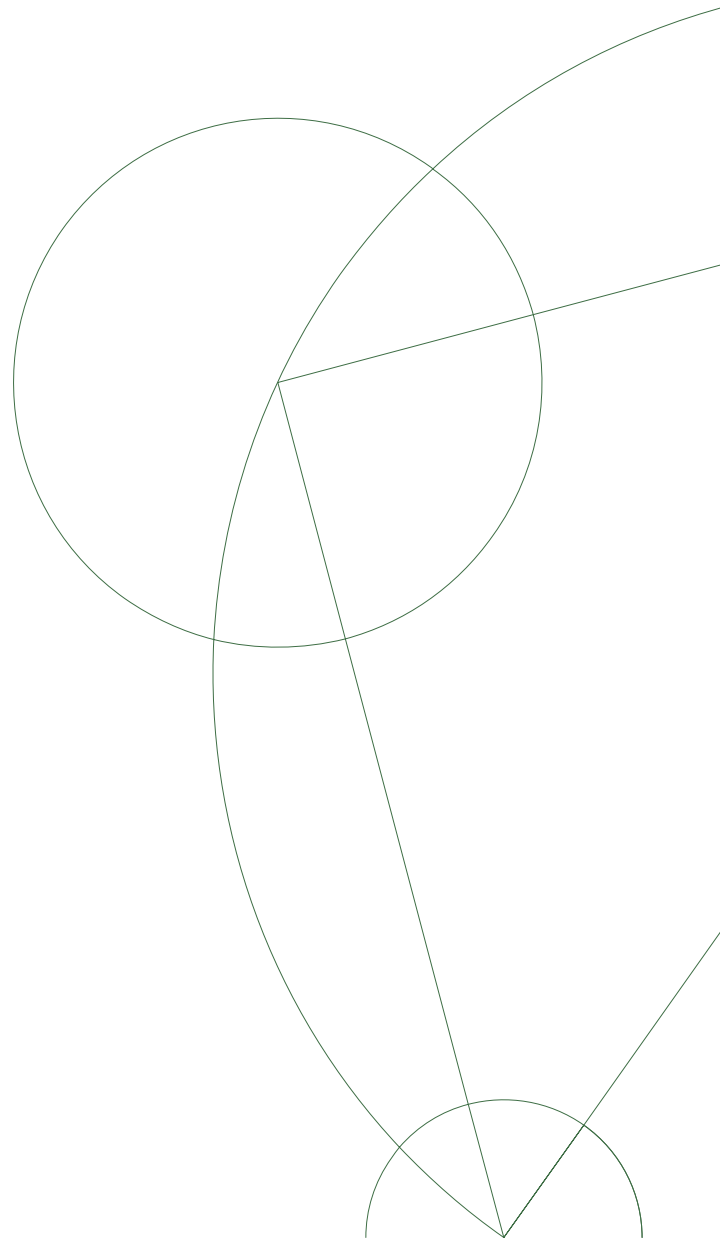
---

Bachelor Project  
Growth and Characterization of LSCO Crystals

Mette Kiehn Grønberg

Supervisors:  
Kim Lefmann & Henrik Jacobsen

Submitted: 11th of June, 2014



# Contents

<b>1</b>	<b>Introduction</b>	<b>1</b>
<b>2</b>	<b>Superconductivity</b>	<b>2</b>
2.1	Zero Resistivity . . . . .	2
2.2	The Meissner-Ochsenfeld Effect . . . . .	3
2.3	BCS Theory . . . . .	4
2.3.1	The Attractive Force . . . . .	4
2.3.2	Cooper Pairs . . . . .	5
<b>3</b>	<b>High Temperature Superconductivity</b>	<b>5</b>
3.1	Cuprates . . . . .	5
3.2	Properties of LSCO . . . . .	6
3.2.1	Introduction to $\text{La}_{2-x}\text{Sr}_x\text{CuO}_4$ . . . . .	6
3.2.2	Structure . . . . .	6
3.2.3	Doping and Phase Transition . . . . .	6
<b>4</b>	<b>Experimental Techniques</b>	<b>8</b>
4.1	Basic Properties of the Neutron and X-ray Scattering . . . . .	8
4.2	Basics of Diffraction from Crystals . . . . .	8
4.3	The Laue Method . . . . .	9
4.3.1	Basic Principle of the Laue Method . . . . .	10
4.3.2	The Laue Spots . . . . .	10
<b>5</b>	<b>LSCO Crystal Growing</b>	<b>10</b>
5.1	Producing LSCO Powder . . . . .	11
5.1.1	Powder . . . . .	11
5.1.2	Mixing . . . . .	11
5.1.3	Heating . . . . .	11
5.2	Producing a Single Crystal . . . . .	12
5.2.1	Creation of Feed and Seed Rods . . . . .	12
5.2.2	Solvents and Seed Rods . . . . .	12
5.2.3	Mirror Furnace . . . . .	13
<b>6</b>	<b>Results and Data Analysis</b>	<b>14</b>
6.1	X-Ray Powder Diffraction . . . . .	14
6.2	X-ray Laue Pictures . . . . .	16
6.3	Neutron Diffraction . . . . .	18
<b>7</b>	<b>Discussion</b>	<b>21</b>
7.1	Summary of Results . . . . .	21
7.2	Discussion of Results . . . . .	22
7.3	Outlook . . . . .	23
<b>8</b>	<b>Conclusion</b>	<b>23</b>
	<b>References</b>	<b>25</b>

<b>A</b>	<b>Appendix</b>	<b>26</b>
A.1	Example of a 100 g batch with doping $x = 0.02$	26
A.2	Example of a 10 g batch for solvents with doping $x = 0.02$	26
A.3	Figures from the data analysis	27
A.3.1	Orient Express	27
A.3.2	Crystal Alignment	28
A.3.3	$x = 0.04$	29
A.3.4	$x = 0.05$	30
A.3.5	$x = 0.06$	32
A.3.6	$x = 0.07$	34
A.3.7	Overview	35



# Abstract

This thesis is a study of how to grow the HTSC cuprate,  $\text{La}_{2-x}\text{Sr}_x\text{CuO}_4$  (LSCO). The Traveling-Solvent Floating-Zone (TSDZ) method was used to produce LSCO crystals. LCO was doped with Strontium, in order to produce LSCO, in the following amounts:  $x = 0.02, 0.03, 0.04, 0.05, 0.06,$  and  $0.07$ . Measurements on the produced crystals have then been performed at Risø-DTU, Denmark and PSI, Switzerland. X-ray diffraction and neutron scattering were used to analyze the crystal structure, in order to determine the quality of the crystals. Several crystals were grown and analyzed by using the methods mentioned. Three of these crystals had single crystal structure. The thesis features a guide on how to grow single LSCO crystals with the use of strontium doping. Even though single crystals were grown, a more standardized method is yet to be developed if single crystals are to be grown more systematically.

## 1 Introduction

Superconductivity (abbreviated S.C.) is a quantum mechanical phenomenon discovered in 1911 by Heike Kamerlingh Onnes [13]. Kamerlingh Onnes saw by chance that when cooling mercury the resistivity suddenly dropped to zero. This observed phenomena caused great interest and opened up a whole new chapter in the history of physics. Since then, a number of elements in the periodic table (mostly metallic elements) have shown superconductivity occurring below a certain critical temperature,  $T_c$ . The value of this critical temperature varies from material to material and is typically in the order of a few kelvins<sup>1</sup>. Unfortunately, achieving temperatures around absolute zero is expensive and limits the technological applications of regular superconductors. Until the recent discovery of superconducting materials operating at temperatures as high as 100+ K, it was not thought to be possible to achieve a high temperature superconductor. These new findings have caused a vast interest in S.C., and scientists hope to one day discover superconductors operating at  $\sim 300$  K. The HTSC theory is still under development as a complete understanding is yet to be found.

These discoveries have also sprouted my interest in this field of research. My thesis concerns the high temperature superconducting cuprate, LSCO. I have grown LSCO crystals with different amounts of strontium doping in order to measure the crystal structure. The single crystal structure is a decisive element in HTSC theory. Even though these LSCO crystals will never be used as superconducting wires, a lot of information about superconductors can still be obtained.

A brief introduction to some of the main aspects of understanding superconductivity and high temperature superconductors are given in section 2 and section 3. The basic experimental techniques used in solid state physics are mentioned in section 4. Section 5 provides a guide to crystal growing and the method used. The main focus has been to analyze the measurements made on LSCO, in order to determine the quality of the crystals, this is shown in section 6 and section 7. Finally in section 8, a conclusion is drawn on basis of the obtained results.

---

<sup>1</sup>Conventional superconductors usually have critical temperatures ranging from around 20 K to less than 1 K.

## 2 Superconductivity

For a material to be considered a superconductor it has to exhibit two distinctive properties when cooled below the characteristic critical temperature: Exactly zero electrical resistance, and expulsion of magnetic fields. The two phenomena will briefly be described in a macroscopic way here, and a further microscopic description will follow in section 2.3.

### 2.1 Zero Resistivity

According to the Drude theory the resistivity in a metal can be written as [1]

$$\rho = \frac{m}{ne^2}\tau^{-1}, \quad (1)$$

where  $m$  is the effective mass,  $-e$  is the charge,  $n$  is the density and  $\tau^{-1}$  is the total scattering rate<sup>2</sup> of the conducting electrons. The scattering rate can be divided into three main processes: Scattering by impurities, by electron-electron interactions and by electron-phonon collisions, written as:

$$\tau^{-1} = \tau_{imp}^{-1} + \tau_{el-el}^{-1} + \tau_{el-ph}^{-1}. \quad (2)$$

Both  $\tau_{el-el}^{-1}$  and  $\tau_{el-ph}^{-1}$  are temperature dependent and proportional to  $T^2$  and  $T^5$  respectively [5]. When the temperature is lowered, the thermal vibrations of the atoms decrease and the conducting electrons are less frequently scattered. However,  $\tau_{imp}^{-1}$  does not have any temperature dependence, and the resistivity at zero temperature depends only on the concentration of the impurities within the crystal.

In a perfect crystal the resistivity will be zero at  $T = 0$  K, otherwise known as a perfect conductor, but such a crystal does not exist. Nevertheless, experiments show that when cooling some materials the resistivity smoothly decreases and suddenly drops to zero below a critical temperature,  $T_c > 0$  K. (See illustration in figure 1) They are said to have passed into the *superconducting state*.

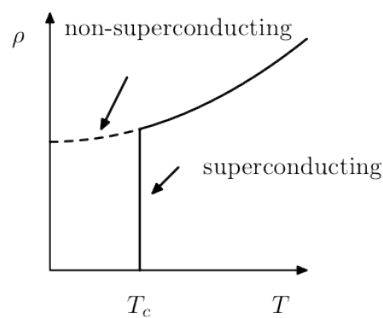


Figure 1: Resistance of a typical material as a function of temperature. The resistance goes to zero at  $T_c$ , and at this temperature the metal becomes superconducting. From [1].

<sup>2</sup>The scattering rate tells how often the particles are being scattered and is given by  $\tau = l/v$ , where  $l$  is the mean free path and  $v$  is the average velocity.

Why some metals turn superconducting at low temperatures is a non-trivial question and will be discussed in section 2.3.

## 2.2 The Meissner-Ochsenfeld Effect

The fact that  $\rho = 0$  is not taken to be the definition of S.C. The fundamental proof that superconductivity occurs in a given material is the demonstration of the Meissner-Ochsenfeld effect [1]. Apart from zero resistivity, when lowering the temperature, the material also becomes a perfect diamagnet [6]. When the diamagnetic material is exposed to an external magnetic field,  $H_{ext}$ , it will expel the magnetic field inside. This happens because the magnetic flux will generate a current,  $I$ , along its surface which exactly cancels out the magnetic field within the S.C.

It can be shown that the magnetic flux (in a S.C.) must stay zero and constant in time - even if  $H_{ext}$  is turned off. However this means that the current (denoted *persistent current*) must also stay constant. If the resistivity in the sample is not exactly zero [1] the current will decay, and from experiments it is shown that the current actually stays finite inside a S.C. However the superconducting state is fragile. If the superconductor is exposed to a large current or a large external field, the material will return to the *normal state*. So there will be a critical current,  $I_c$ , and a critical field,  $H_c$ , for which the superconductor will become a normal metal above this value [1].

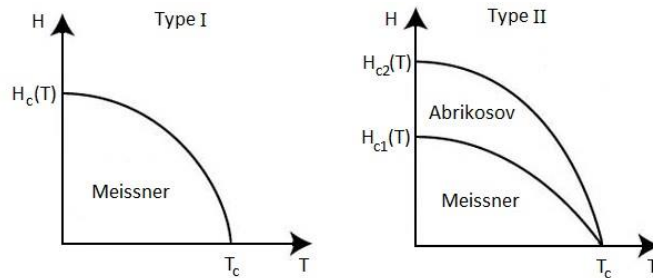


Figure 2: *Difference between **Type I** and **Type II** superconductors. The superconducting phase in **Type I** and below  $H_{c1}$  in **Type II** is called Meissner phase because  $\mathbf{B} = 0$  inside the superconductor. Abrikosov is the phase in between  $H_{c1}$  and  $H_{c2}$  in Type II, where  $\mathbf{B} \neq 0$  inside the sample as  $H_{ext}$  enters the superconductor. From [1].*

Superconductors are classified into two types; **Type I** and **Type II** superconductors and are based on the response when a material is exposed to an external magnetic field. In a **Type I** superconductor, the magnetic field,  $\mathbf{B}$ , inside the sample remains zero, until  $H_{ext}$  reaches a certain critical value,  $H_c$ . At that point the superconductivity instantly breaks down, and the sample returns to the normal metal phase. The superconducting phase is called the *Meissner phase*. However, in a **Type II** superconductor the situation is different. When  $\mathbf{H} = 0$ , the superconductor is in the Meissner phase and the  $\mathbf{B}$  field inside the sample is still zero. The  $\mathbf{B}$  field remains zero for an increasing  $\mathbf{H}$  field, until it reaches a lower critical field,  $H_{c1}$ . The superconductor will then turn to the *Abrikosov phase*. In this phase, the magnetic flux is able to enter the superconductor as vortices [1], and in these vortices the superconductivity will be

destroyed. All around the vortices, the superconductivity will stay intact, and it will continue to do so until it reaches an upper critical field,  $H_{c2}$ . At  $H_{c2}$  the superconductivity will be completely destroyed. A phase diagram as a function of temperature and the varying fields is shown in figure 2.

## 2.3 BCS Theory

The BCS theory was published in 1957 by Barden, Copper and Schrieffer (BCS) and is a microscopic theory of superconductivity [2]. It describes the conceptual and mathematical foundation and is generally accepted to be the correct theory of conventional superconductivity [1]. The complete microscopic theory of S.C. is extremely complicated, and requires an advanced knowledge of quantum mechanics [2]. I will not try to cover the entire BSC theory, but only give some important aspects required in order to understand S.C.

The main idea behind the BSC theory is that electron-phonon interactions will create an effective attraction between electrons near the Fermi surface. It may seem surprising to find an attractive force, because electrons obviously repel each other strongly with the Coulomb repulsion. In the case of S.C. the effective attraction is caused by slow moving positive ions in the medium and the electron-ion potential simply overwhelms the repulsive electron-electron interactions leading to a net attraction. As a result electrons are coupled together in Cooper pairs, the carriers of the *super current*. See figure 3.

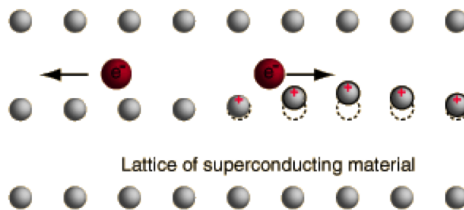


Figure 3: The figure shows the moving electrons within the lattice. The negative electron attracts the positive ions. The lattice movement is delayed and the positive region created behind the first (left) electrons attracts the second (right) electron. From [15].

### 2.3.1 The Attractive Force

To be more accurate, the attractive force between the electrons arises from the Pauli exclusion principle and screening effect. Let us consider an electron traveling with momentum  $\hbar\mathbf{k}_1$  within a metallic environment. The electron will interact with the crystal lattice and hence the electron can excite a phonon with momentum  $\hbar\mathbf{q}$ , producing an electron with momentum  $\hbar\mathbf{k}'_1 = \hbar\mathbf{k}_1 - \hbar\mathbf{q}$ . This phonon will eventually be absorbed by another electron and the electron gains the momentum carried by the phonon and ends up with momentum  $\hbar\mathbf{k}'_2 = \hbar\mathbf{k}_2 + \hbar\mathbf{q}$ . The interaction can be drawn as a vertex of a Feynman diagram, as shown in figure 4.

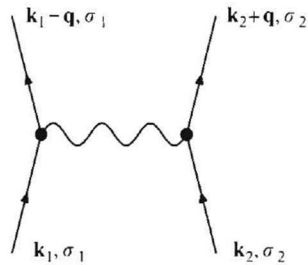


Figure 4: Feynman diagram of an electron-electron interaction at the Fermi surface due to exchange of crystal lattice phonons. From [1].

The electrons still experience a coulomb repulsion and the net interaction is determined by the relative magnitude of the phonon energy  $\hbar\omega$  and the energy difference between the initial and final states of the electrons. When the attractive energy is larger than all the contributions to the effective repulsive energy, a bonding between the electrons is possible. For a bonding to occur the phonon frequency has to be less than the Debye frequency,  $\omega_D$ , and it is only electrons within the energy range  $\pm\hbar\omega_D$  of the Fermi surface that are involved in the interactions.

### 2.3.2 Cooper Pairs

The attractive force results in highly correlated pairs of conducting electrons formed below  $T_c$ . The fact that electrons condensate into the same state is against all previous assumptions of allowed electron behavior. Electrons are fermions and cannot occupy the same state due to the Pauli exclusion principle. But the electrons in the Cooper pairs are bound together in pairs with equal but opposite spin and momentum ( $\mathbf{k} \uparrow, -\mathbf{k} \downarrow$ ) which lead to the net spin of a pair becomes zero. This means that the pairs behave like bosons. Bosons do not obey the Pauli exclusion principle and they can all condensate into the same state. This allows the Cooper pairs to condensate into the lowest possible energy state. The pairing electrons result in a small gap  $2\Delta$  separating the occupied and unoccupied states near the Fermi surface. The  $2\Delta$  corresponds to the energy for breaking up a pair into two free electrons and was first predicted by the BCS theory [1].

## 3 High Temperature Superconductivity

In this chapter I will introduce the high-temperature superconductor (abbreviated HTSC) oxides also known as cuprate superconductors, as well as an introduction to the cuprate LSCO and its properties.

### 3.1 Cuprates

The first high- $T_c$  superconductor was discovered in 1986 by Bednorz and Müller [12] and for this they were awarded the Nobel Prize in Physics in 1987. They found that certain metal oxides showed superconducting behavior at unusually high temperatures. Ordinary or metallic

superconductors usually have transition temperatures below 30 K whereas HTSC have been observed with transition temperatures as high as 138 K [].

Metal oxides or cuprates are **Type II** S.C. and are in general highly anisotropic<sup>3</sup> antiferromagnetic insulators with no tendency of superconductivity. Cuprates differ from regular S.C. by having a multi-layered crystal structure that consists of quasi-two-dimensional copper-oxygen (CuO<sub>2</sub>) planes and superconductivity essentially takes place within these planes [13]. The superconducting phase is achieved by removing or adding electrons from the CuO<sub>2</sub> planes. This can be done by adding/doping with either alkaline earth ions (like Ba, Sr, Zn) or oxygen [3]. Doping the HTSC materials destroys the antiferromagnetic long-range ordered state [12] and reduces the insulating behavior and allows the existence of the Cooper pairs.

## 3.2 Properties of LSCO

### 3.2.1 Introduction to La<sub>2-x</sub>Sr<sub>x</sub>CuO<sub>4</sub>

La<sub>2</sub>CuO<sub>4</sub> (LCO) is the parent compound of La<sub>2-x</sub>Sr<sub>x</sub>CuO<sub>4</sub> (LSCO), where  $x$  is referred to as the doping value, which is equal to the hole concentration per Cu atom in the CuO<sub>2</sub> plane [12]. Undoped LCO is highly antiferromagnetic and exhibits no superconducting properties. Like any other cuprate La<sub>2</sub>CuO<sub>4</sub> consists of a sequence of evenly spaced CuO<sub>2</sub> sheets separated by regions containing oxygen and lanthanum.

### 3.2.2 Structure

LCO has a tetragonal<sup>4</sup> crystal structure for temperatures above 500 K [11]. When lowering the temperature the crystal transforms into an orthorhombic<sup>5</sup> lattice structure [11] where the  $a$  and  $b$  axes span the CuO<sub>2</sub> planes and  $c$  denotes the interplanar lattice constant. See figure 5 (left).

The same transition applies for the doped daughter compound LSCO, but the transition temperature depends on the amount of doping (Sr<sup>2+</sup>). Around 300 K LSCO occurs in the form of the orthorhombic structure in the doping range of 0 – 0.1 See figure 5 (right). In La<sub>2</sub>CuO<sub>4</sub> the unit cell contains two CuO<sub>2</sub> sheets with a spacing of  $c \approx 13.15$  Å,  $a \approx 5.36$  Å and  $b \approx 5.41$  Å for  $x = 0.00$  [9]. The exact values of  $a$ ,  $b$  and  $c$  depend of the doping. When the amount of doping increases, the difference between  $a$  and  $b$  decreases thus moving LSCO towards to the tetragonal structure. Since we are working at room temperature  $\approx 300$  K and within the doping range of 0.02 to 0.07, our only concern is the orthorhombic structure.

### 3.2.3 Doping and Phase Transition

The superconducting effect in La<sub>2</sub>CuO<sub>4</sub> is basically achieved by substituting Sr<sup>2+</sup> ions for La<sup>3+</sup> ions. To maintain the charge balance, 2 electrons are removed from the CuO<sub>2</sub> planes which changes the electron configuration of the Cu ions (2+) from [Ar]3d<sup>10</sup>4s<sup>1</sup> to an incomplete d shell

---

<sup>3</sup>Unequal physical properties along different axes. In contrast to isotropic which implies identical properties in all directions.

<sup>4</sup>Tetragonal structure:  $a = b \neq c$ ,  $\alpha = \beta = \gamma = 90^\circ$

<sup>5</sup>Orthorhombic structure:  $a \neq b \neq c$ ,  $\alpha = \beta = \gamma = 90^\circ$

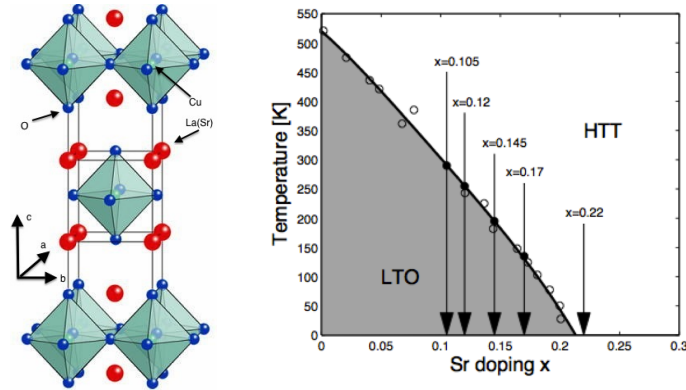


Figure 5: *Left: The tetragonal crystal structure of undoped LCO. The red, blue and green orbs represent the La(Sr), Cu and O ions respectively. From [16]. Right: LSCO phase diagram showing the transition between the tetragonal (HTT) and orthorhombic (LTO) phase. From [3].*

with only 9 electrons [11]. The missing electrons (holes) are mobile and below  $T_c$  they can form Copper pairs.

For applications, of HTSC a high  $T_c$  is favorable. Apart from the type of material, the critical temperature depends on both the concentration of doped ions and the number of CuO<sub>2</sub> layers. The more layers of CuO<sub>2</sub> the higher  $T_c$ , however, the answer is not straightforward in relation to the concentration of doping.

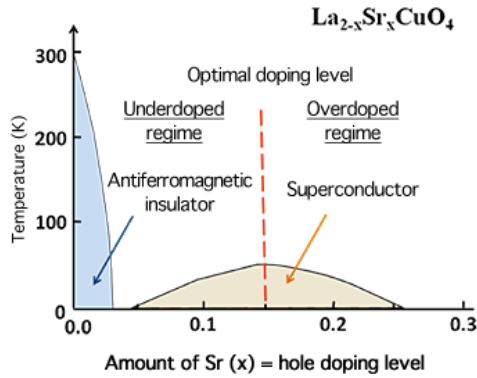


Figure 6: *The phase diagram of LSCO as a function of Sr doping. LSCO is an insulator from  $x \lesssim 0.05$  for  $0 < T < 300$  K, superconductor from  $0.05 \lesssim x \lesssim 0.16$  with an increasing  $T_c$ . The optimal doping level is at  $x = 0.16$  where the highest  $T_c$  is reached. LSCO is still a superconductor from  $0.16 \lesssim x \lesssim 0.25$  with an decreasing  $T_c$ . There exists an (IC) magnetic order in the superconducting phase as well as in the "gap" between the two phases (from insulator to superconductor) at  $x = 0.03$  to  $x = 0.05$ . From [17].*

At  $T = 0$  K without doping ( $x = 0$ ) LSCO is in its normal state (recall antiferromagnetic and insulating), but adding a finite small amount of doping takes LSCO into the superconducting

state still at  $T_c \approx 0$ . As the amount of doping is increased the superconducting transition temperature  $T_c$  rises until it reaches a maximum value  $T_c^{max}$ . The doping value at this point is called the *optimal doping level*. However, a further increase of  $x$  makes  $T_c$  decrease until a finally critical amount of doping is reached and the normal state is yet again favoured. See figure 6. The optimal doping for LSCO is  $x = 0.16$  with  $T_c \sim 38$  K [3].

## 4 Experimental Techniques

Experimental techniques, such as x-ray scattering, neutron scattering, electron microscopy and nuclear magnetic resonance (NMR) are often needed in order to fully understand the structural properties of a material. The various experimental techniques often complement each other when applied on the same material, which is why they are rarely used separately.

### 4.1 Basic Properties of the Neutron and X-ray Scattering

The development of the *neutron scattering technique* has proved to be a major asset when studying condensed matter in general and superconductors in particular. Neutrons interact with matter through the strong force and electromagnetic force. By using the neutron scattering techniques it is possible to determine the position and motion of the atoms. This is done by studying the interaction that occurs between the scattered neutron and the nuclei due to the strong force. The neutron's magnetic interaction with the electrons allows magnetic structures and excitations to be investigated.

The free neutron does not exist naturally in nature. Once it is outside the nuclei it will  $\beta$  decay with a lifetime,  $\tau = 886$  s ( $\sim 15$  min.). Nevertheless, this lifetime is long enough for neutron scattering experiments to be performed [4]. The neutron carries zero electrical charge, but its constituent quarks each have an independent charge, which causes the neutron to possess a weak magnetic moment:

$$\mu = \gamma\mu_N, \tag{3}$$

where  $\gamma = -1.913$  is the neutron magnetogyric ratio, and the nuclear magneton is given by  $\mu_N = e\hbar/(2m_p)$ . Zero net charge means that the neutrons are not affected by the Coulomb repulsion. This means that the neutrons can travel large distances through most materials without being scattered or absorbed, and once they do interact they are only weakly scattered. Neutron's ability to penetrate a sample makes it possible to measure if the average properties are homogeneous distributed through the bulk of the crystal and not just in the surface layers. This gives neutrons an advantage over x-ray scattering, where often only the surface of the material is probed. However, the neutron technique is slow and expensive and should only be used where other methods are inadequate [4].

### 4.2 Basics of Diffraction from Crystals

When studying the scattering from a crystal lattice, one will find that only scattering from certain angles (at fixed wavelength) will exhibit constructive interference. To be more accurate

the scattering has to fulfill the Bragg law. Bragg's law is a consequence of the periodicity of the lattice and given by [5]:

$$n\lambda = 2d\sin(\theta), \quad (4)$$

where  $n$  is an integer,  $\lambda$  is the wavelength of the incident beam,  $d$  is the spacing between the planes in the atomic lattice, and  $2\theta$  is the angle between the incident and diffracted beam, see figure 7. However, it is important to note that scattering will only occur if  $\lambda$  is less than  $2d$ .

In physics it is convenient to define the *reciprocal lattice vector*:

$$\mathbf{G} = h\mathbf{a}^* + k\mathbf{b}^* + l\mathbf{c}^*, \quad (5)$$

where  $(h, k, l)$  are integers denoting the lattice plane and  $\mathbf{a}^* = \mathbf{b} \times \mathbf{c} / \mathbf{a}(\mathbf{b} \times \mathbf{c})$ , and similar for  $\mathbf{b}^*$  and  $\mathbf{c}^*$ .

Furthermore, we define the scattering vector,  $\mathbf{q}$  as:

$$\mathbf{q} = \mathbf{k}_i - \mathbf{k}_f. \quad (6)$$

In order for scattering to occur the Laue condition,  $\mathbf{q} = \mathbf{G}$  must be fulfilled and from  $\mathbf{q} = \mathbf{k}_i - \mathbf{k}_f$  we can derive that:

$$G = 2k\sin\theta, \quad (7)$$

which is equivalent with Bragg's law.

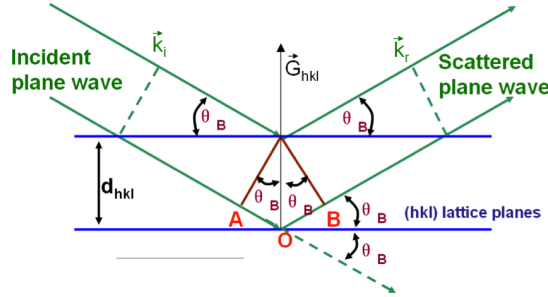


Figure 7: The figure illustrates Bragg's law and the Laue condition. From [18].

Neutrons can be scattered in two different ways: *elastic scattering* and *inelastic scattering*. Elastic scattering is mainly used for determining crystal structures while inelastic scattering is used in the study of atomic excitations. In elastic neutron scattering all the kinetic energy from the particle is conserved in contrast to inelastic scattering. The neutron scattering method used in our experiments was based on elastic scattering, see section 6.

### 4.3 The Laue Method

The Laue method is an x-ray imaging technique for crystals based on Bragg diffraction. It creates a two-dimensional intensity mapping of the beam diffracted by a crystal and can be used to analyze crystal structures and orientations as well as in the study of crystalline imperfections. The short penetration depth of x-rays limits the analysis to the surface of the crystal. For further investigation neutron scattering is the desired tool.

### 4.3.1 Basic Principle of the Laue Method

An incident beam of continuous wavelength within the x-ray bandwidth (also known as a white beam) is directed to strike on a fixed single crystal. The Bragg angle,  $\theta$ , is then fixed for every set of planes in the crystal, and each set picks out and diffracts the wavelengths that satisfy the Bragg law. Diffraction gives rise to a reflected beam, which will leave the crystal and propagate along a direction differing from the incident direction by the scattering angle  $2\theta$  (from Bragg's law). There are two basic methods regarding Laue diffraction depending on the relative position of the source, crystal and the image plate (photographic film).

In the *transmission Laue method* (the original Laue method) an image plate is located behind a crystal to record the beams diffracted in the forward direction. The method is called transmission method, because the diffracted beam is transmitted partially through the crystal.

The second method is the *back-reflection Laue method* where the image plate is placed between the beam and crystal. The image plate has a hole in the middle where the incident beam passes through. The beam is then diffracted in a rearward direction and recorded.

### 4.3.2 The Laue Spots

The recorded diffracted beam will show up as an array of spots forming a pattern on the image plate. These spots correspond to the intensity peaks from the Bragg diffraction. The created pattern will have some kind of symmetry corresponding to the symmetry of the crystal and the directions of the crystal axes are therefore determined by the symmetry axes of the pattern. The pattern is like a fingerprint and unique for every crystals. An example of a Laue picture is given in figure 8. More examples of Laue pictures of our LSCO crystals are shown in section 6.2.

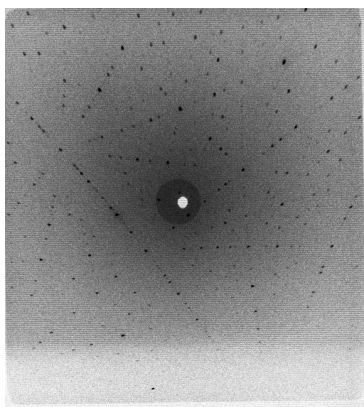


Figure 8: A Laue picture of the  $x = 0.05$  crystal. The black spots mark the intensity from the backscattered Bragg peaks, and the white circle in the middle shows the center of the beam.

## 5 LSCO Crystal Growing

In this chapter, the growth of LSCO single crystals by the *Traveling-Solvent Floating-Zone* (TSFZ) method is described. As mentioned in section 3 doping is the crucial element needed for

the occurrence of superconductivity in the LSCO cuprate. The optimal doping with strontium ions  $\text{Sr}^{2+}$  is  $x = 0.16$  which will yield the highest  $T_c$ . The exact amount of doping, and the interval of  $x = 0.10$  to  $x = 0.18$ , have been extensively studied beyond recognition, but little attention has been paid to the lower doping limit of the superconducting state. Beliefs are that a correlation between magnetism and superconductivity might exist, even at a lower doping limit. Which is why studying crystals at lower  $x$ 'es, for instance  $x = 0.05$  to  $x = 0.07$ , is interesting. In my work at DTU, Risø campus, Denmark (denoted Risø in this thesis), LSCO crystals with doping  $x = 0.02, 0.03, 0.04, 0.05, 0.06$  and  $0.07$  have been grown.

The practical steps towards producing a single crystal from LSCO powder are briefly summarized below. The LSCO crystals are initially made from compounds of powder, which are carefully mixed. The powder is then heated before being compressed into a cylindrical rod. The rod is sintered in order to create a feed rod and a seed rod. The produced rods are then melted in a mirror furnace in order to create single crystals. A more thorough explanation of each step is given in the following subsections.

## 5.1 Producing LSCO Powder

### 5.1.1 Powder

Copper (II) oxide ( $\text{CuO}$ ), strontium carbonate ( $\text{SrCO}_3$ ) and lanthanum (III) oxide ( $\text{La}_2\text{O}_3$ ) were used in order to produce LSCO. The ratio of the amount of  $\text{CuO}$  and  $\text{Sr}$  ions to the amount needed in a complete reaction of  $\text{La}_2\text{Sr}_x\text{CuO}_4$  was balanced in such a way that there was a redundant amount of 3 mol%  $\text{CuO}$  and  $x$  mol%  $\text{Sr}$  ions. This gives the following reaction scheme:  $1.03 \text{ CuO} + (2-x)/2 \text{ La}_{2-x}\text{O}_3 + x \text{ Sr}_x\text{CO}_3 \rightarrow \text{La}_{2-x}\text{Sr}_x\text{CuO}_4$ . If the reaction is not complete, the crystal produced will not be a single crystal.

The molar masses and specific calculations of a batch is shown in appendix [A.1](#).

### 5.1.2 Mixing

The three components ( $\text{CuO}$ ,  $\text{SrCO}_3$  and  $\text{La}_2\text{O}_3$ ) of the batch were each carefully weighed and mixed in a glove box with an argon overpressure of approximately 10 mbar. The argon atmosphere prevents the powder from reacting with the air and since argon is a noble gas it will not react with anything. After the batch was mixed it was held in a closed container and placed in a shaker for 24 hours to make sure that it had been properly mixed.

### 5.1.3 Heating

The powder was poured into an aluminum oxide container and calcined at  $950^\circ\text{C}$  for two days. The high temperature allows the  $\text{La}_2\text{O}_3$  to react with  $\text{SrCO}_3$  and  $\text{CuO}$  and produce  $\text{LaSrCuO}_4$ . Once the powder was calcined, it was manually crushed with a pestle and mortar in order to remove any inhomogeneities. The entire routine was then repeated. When the powder is newly mixed, it has a light gray color<sup>6</sup>, but after each heating the color becomes a darker gray. This change in color is a good indicator of LSCO having been produced. Quality control of the powder is to be done by x-ray diffraction and the results can be seen in section [6.1](#).

---

<sup>6</sup>The initial gray color comes from mixing  $\text{SrCO}_3$  (black) with  $\text{CuO}$  and  $\text{La}_2\text{O}_3$  (white). LSCO is black colored.

## 5.2 Producing a Single Crystal

### 5.2.1 Creation of Feed and Seed Rods

The twice-calcined powder was then again crushed in the mortar. Afterwards the powder was packed into a silicon tube and both ends were then sealed. It is important that the powder is tightly packed with no air lumps in it, since any air trapped inside will potentially cause the crystal to crumble when calcined. The sealed silicon tube was then coated in a condom and the air was removed with a vacuum pump. The condom protects the powder from getting wet later on in the process. The silicon tube and condom were then both placed in a close fitting copper tube to help keep the silicon tube straight during the compression phase.

The copper tube was placed into an iron container, which was then filled with water, before being moved to a hydrostatical pressure machine. The machine works by pressing a cylindrical lid down in the iron container, forcing a large pressure on the water and tube. Since water has a very low compressibility<sup>7</sup>, and will not be compressed much, the powder is pressed tight together instead.

The machine was configured to build up a pressure of 90 kp/cm<sup>2</sup> (corresponding to approximately 40 tons) for 5 minutes. When the rod had been compressed it measured approx. 0.6 cm in diameter and 8 to 10 cm in length depending on the length of the silicon tube. Immediately after compression, the rod was placed in a specially designed vertical furnace (oven) and calcined for two days at 1100 °C. The vertical oven helps straighten the rod. If the rod is not sintered immediately after compression it will begin to crumble and fall apart within a few hours.

### 5.2.2 Solvents and Seed Rods

Solvents are small disk-shaped pills with an extremely high content of copper oxide. They play an important role in the TSFZ method. The solvents were produced in the same way as the rods. They were doped with the same amount of Sr<sup>2+</sup> but the difference was a high content of CuO. According to some literature [8] the solvents should contain 78-80 mol% of CuO. We have chosen 80 mol% of CuO which gives us 0.8 parts CuO and 0.2 of La<sub>2-x</sub>Sr<sub>x</sub>CuO<sub>4</sub>. The solvent was used to launch and facilitate the crystal growing process. In brief, the solvent lowers the melting point of the powder and thereby eases the entire process. A more complete explanation of the properties of solvents is not given in this thesis. Read [7] for further information. See calculations of a batch of solvents in appendix A.2.

When using the TSFZ method a seed rod (or a LSCO crystal) is required in order for the crystal to have something to grow on to. The seed rod is equivalent to the feed rod but has a length of approx. 2 cm. It can be produced by the exact same procedure as the feed rod, or if the feed rod is long enough, a piece can be cut off. The solvent and seed rod are both used in the mirror furnace as described in the following section.

---

<sup>7</sup>Compressibility is the fractional change in volume per unit increase in pressure. For each atmosphere increase in pressure, the volume of water would decrease 46.4 parts per million.

### 5.2.3 Mirror Furnace

The last step of the process of growing a single crystal takes place in the mirror furnace. Inside the oven the main rod was melted in order to grow it into a single crystal. At this point the rod consists of LSCO crystals oriented in all directions, but melting it in the mirror furnace should orientate the crystals in one direction. The furnace itself consisted of four ellipsoidal mirrors, equipped with a halogen lamp at the center of each mirror. Platinum wires in a ceramic hollow container supported the seed rod and the solvent was glued on top of it. The feed rod was held in place by a wire and placed above the solvent with a few millimeters of spacing. Both the feed rod and the seed rod were placed in such a way that the solvent initially was positioned in the middle of the mirrors. See figure 9 for a schematic illustration and a picture from inside the mirror furnace.

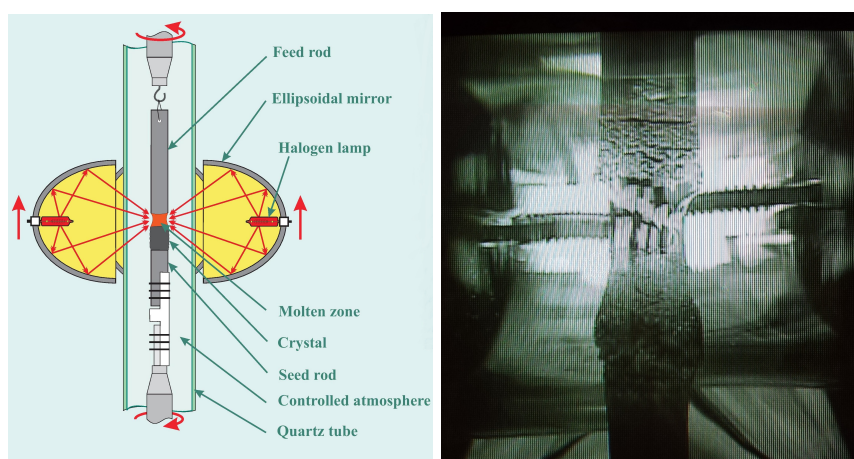


Figure 9: *Left: An illustration of the mirror furnace. The various elements are plotted in the figure. Right: Real picture of the working furnace. A stable molten zone is maintained.*

The principle of the TSFZ technique is to melt a small section of the feed rod by radiating light on to it by means of the mirrors. Initially the mirrors were placed in such a way that the focused light would target the solvent. As the temperature was raised the solvent melted and the feed rod was moved down to join the solvent. By moving the mirror upwards the molten (floating) zone would travel along the length of the feed rod. As the mirrors moved upwards the floating zone solidified on the seed rod and crystallization occurred in the solidification process.

The speed of the mirrors, hence the growth speed, and the temperature both play a major part in establishing a steady state. If the temperature is too high the melting zone will drain away or collapse. If on the other hand the temperature were too low the melting zone would risk to solidify, which would then be seen as small grains in the molten zone. Both the temperature and melting rate depends on the material and the dimensions of the rod.

We were growing at a rate of 1 mm per hour, suitable for a 0.6 cm diameter rod. In order to stabilize the molten zone, the feed and seed rods were rotated in opposite directions at a rate of 30 rpm.

The rod system is located within a sealed quartz tube, which gives the opportunity to

grow crystals in different atmospheres. The high temperature causes copper to evaporate and escape from the molten zone. If copper is missing in the process the crystallization will not form properly. By introducing oxygen pressure, copper atoms are more likely to stay inside the molten zone. In our case we were not able to use this advantageous element and instead the rods were doped with 3% mol CuO.

Results and a discussion from the crystal growing process is shown in section 7.1 and 7.2 and the masses of the crystals are shown in table 2 in appendix A.3.2.

## 6 Results and Data Analysis

This section contains the results and analysis of the measurements made on the crystals. The first and most vital element in the analysis is to determine whether the crystals that have been grown are single crystals or not. This will be the main focus in this analysis. Two problems however, are that if the HTSC material is not a 'pure' single crystal or twinned<sup>8</sup>, we are not able to obtain good and usable experimental results on subsequent experiments, as discussed in section 7.3. A variety of methods and measurements exist in order to describe the different properties of the crystals. Each of these methods has its own purpose and benefits. In my analysis I have used three different methods: X-ray diffraction; to determine the content of LSCO powder, crystal powder and solvents, the Laue method; initially used to look at the surface structure and later for alignment as preparation for neutron scattering, the neutron scattering technique; used to investigate the bulk of the crystal by measuring intensity of individual peaks and grid scans.

### 6.1 X-Ray Powder Diffraction

One way to examine the contents of the heated LSCO powder is by using the x-ray powder diffraction method explained in section 4.2. This can be used as a *quality control* since it will reveal any unreacted elements or unintended reactions. As mentioned in section 5.1.1 a crucial element when growing single crystal is that the reaction is complete. Therefore x-ray diffraction is used in order to determine whether the reactions have occurred properly or not.

To analyze the data the program FullProf [10] was used. Intensity peaks occur from the Bragg reflections and FullProf models the peak as Voigt profiles<sup>9</sup> on the basis of the cell parameters of the crystal and the compounds from possible reactions.

From the known contents of the sample, FullProf is then able to compute the scattering signal, while optimizing several parameters; the most important of these is the relative amount of scattered photons. Ideally, the quality control should have been done for every powder and crystal but because of technical problems this was not done. Listed below are four measurements showing the sample content.

Measurements from powder with  $x = 0.07$  reveal a content of 7.09 mol%  $\text{La}_2\text{O}_3$  + 92.91 mol% LSCO. The powder was mixed before the method with the extra CuO was launched and that is why we don't see 3 mol% of CuO as explained in section 5.2.3. The high content of  $\text{La}_2\text{O}_3$

---

<sup>8</sup>Twinning means that the  $a$  and  $b$  axes are reversed.

<sup>9</sup>The Voigt profile is a line profile used in spectroscopy and diffraction, and consists a convolution of a Gaussian and a Lorentz profile. In practice this is often approximated by a sum of a Lorentzian and a Gaussian.

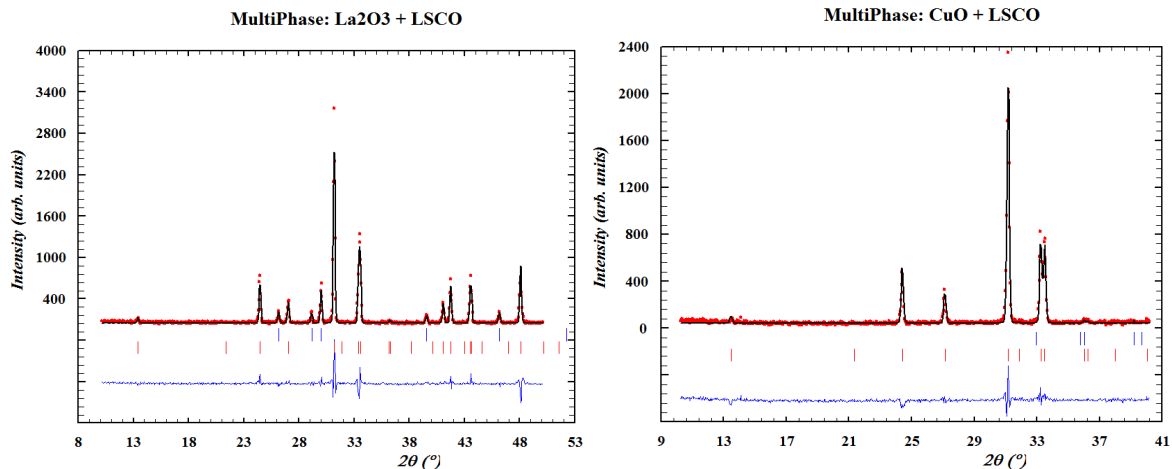


Figure 10: The  $\text{La}_2\text{O}_3$  and LSCO intensity distribution from  $x = 0.07$  (left) and the CuO and LSCO intensity distribution from  $x = 0.02$  (right). Shown in red are the data points measured with x-ray diffraction. The black line is a fit made in FullProf. The blue line shows the difference between the calculations and the measurements. The red and blue vertical lines shows the positions of Bragg peaks, with LSCO (red) and  $\text{La}_2\text{O}_3$  (blue) to the left, and LSCO (red) and CuO (blue) to the right. The CuO peaks are small and not clearly visible on the figure to the right.

might indicate a miscalculation, but this has not seemed to be the case. The result of the data analysis from FullProf can be seen in figure 10.

The FullProf analysis shows that the powder contains only LSCO and  $\text{La}_2\text{O}_3$  (left), and LSCO and CuO (right) respectively. This can be concluded since the fitted intensity peaks appear at the same angles as the measured peaks. FullProf uses the known contents of the powder, to predict the location of the intensity peaks.

The line showing difference between data and fit shows some variation. A perfect fit would appear as a straight line, and any variations between data and fit would be shown as oscillations. The shown difference between data and fit may be due to the fact that FullProf fits using a Voigt profile might not be the exact mathematical function for describing diffraction. However, though a straight line would be ideal, it is equally important that the peaks of the line, indicating difference between fit and data, occurs at the same angles as the intensity peaks. This indicates that FullProf correctly identifies all intensity peaks, and that the difference shown lies in the shape of the fitted line alone. This means that the sample is most likely LSCO and  $\text{La}_2\text{O}_3$  (left).

Overall, one of the biggest challenges in the crystal growing process is unreacted  $\text{La}_2\text{O}_3$  in the crystals. Therefore, as an experiment, we have tried to mix the unheated powder with  $x = 0.02$  in ethanol ( $\text{CH}_3\text{CH}_2\text{OH}$ ) instead of the 24-hours shaking. The ethanol will not react with the powder itself and the intention is that the compounds in the powder will be more equally distributed before heating. Shown in figure 10 (right) are our results with the ethanol-based method.

The results from the ethanol-based method shows that after heating, the powder consists

of 3.31 mol% CuO + 96.69 mol% LSCO. This is close to the intended dose of 3.00 mol% CuO + 97.00 mol% LSCO. Unfortunately we failed to grow a single crystal from this powder. The feed rod was subjected to too much heat, and a stable melting zone was not maintained for long enough. As a result of this, the experiment was aborted and a single crystal was not further produced for this doping. It appears reasonable to conclude that the ethanol-based method seems to work better, even though the method might not prove to be an easier way to produce pure crystals.

A third powder diffraction measurement was done on the crystal with  $x = 0.03$ . The crystal was left out in the air and within a week it started to crumble. The measurement was then done on some of the crumbled powder. It showed that the content of the powder consisted of 46.00 mol% LSCO and 54.00 mol%  $\text{La}(\text{OH})_3$  (lanthanum(III) hydroxide). The  $\text{La}(\text{OH})_3$  was produced when unreacted  $\text{La}_2\text{O}_3$  reacted with  $\text{H}_2\text{O}$  from the air. And it was the high content of  $\text{La}(\text{OH})_3$  which caused the crystal to crumble. If the crystal had contained 100 mol% LSCO it would have remained intact, since LSCO is not affected by the air.

The fourth measurement shows that the content of a solvent with  $x = 0.04$  is 78.10 mol% CuO and 21.90 mol% LSCO. The intended content was 80 mol% CuO and 20 mol% LSCO and this result gives us an estimate of how much we have actually produced. To explain the difference from the intended content the accuracy of FullProff has to be included. The accuracy of FullProff is not informed, but my estimate is 1.0. Furthermore the accuracy of the weighing is worth to consider, even though the error might be negligible.

## 6.2 X-ray Laue Pictures

In order to examine the surface structure of the crystal Laue pictures were taken at Risø. This way it is possible to get a preliminary idea of the quality of the crystals before a more thorough and expensive examination was to be done. Figure 12 shows the Laue pictures taken at Risø of the  $x = 0.04$  crystal.



Figure 11: Pictures of  $x = 0.04$ . Three different measurements on the same crystal are shown. The red spot marked the striking point of the beam.

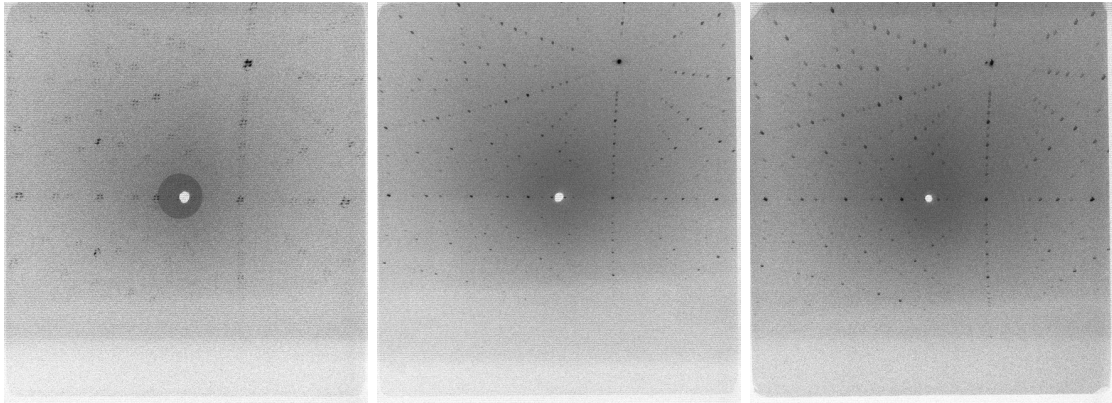


Figure 12: *Laue pictures of  $x = 0.04$ . The three Laue measurements shown in this figure correlates to the three pictures in the figure above. The black spots mark the intensity from the backscattered Bragg peaks, and the white circle in the middle shows the center of the beam. It is evident that the three Laue measurements are similar when measuring along the longitudinal axis of the crystal.*

The figure shows that the same Laue patterns appear when measuring in three different spots along the longitudinal axes of the crystal. This indicates that the surface structure might be homogeneous.

It is difficult to use Laue in order to directly determine the structure of an unknown crystal. It is however possible to simulate Laue diffraction from LSCO, as shown later on in figure 13. This fact implies that the structure created with out any doubt is LSCO crystals. The only question remaining is the quality and homogeneity of the structure. Furthermore it is possible, by looking at the quality of the pattern, to reveal impurities or twinning. If the crystal is twinned the peaks will be adjacent and close together. On the Laue pictures the peak would appear as doubled dots with only a small displacement.

For gathering further information about the crystals from the Laue pictures the program Orient Express [14] has been used. Orient Express needs the parameters from LSCO unit cell and the high symmetry spots from the pattern. From this information it is able to make a fit of the spots and calculate from which plane each single point has been reflected. By labeling the spot/planes it is possible to determine the directions of the axes. See figure 13. The figure shows that the  $c$ -axis is not along the longitudinal axis. See fits from  $x = 0.05$  and  $x = 0.07$  in appendix A.3.1. A more complete study of the orientation of all the crystals is shown in the next section.

More Laue pictures from  $x = 0.02$ ,  $0.04$ ,  $0.05$  and  $0.06$  were taken at Risø, but only some of the pictures of  $x = 0.04$  are included this thesis. Here is a quick overview of the results of them all.  $x = 0.02$  showed low intensity peaks and signs of twinning,  $x = 0.04$ ; 2 out of 5 pictures showed low intensity peaks, the rest looked normal,  $x = 0.05$ ; all 5 pictures looked normal,  $x = 0.06$ ; showed irregularities in all 8 pictures and sign of twinning.

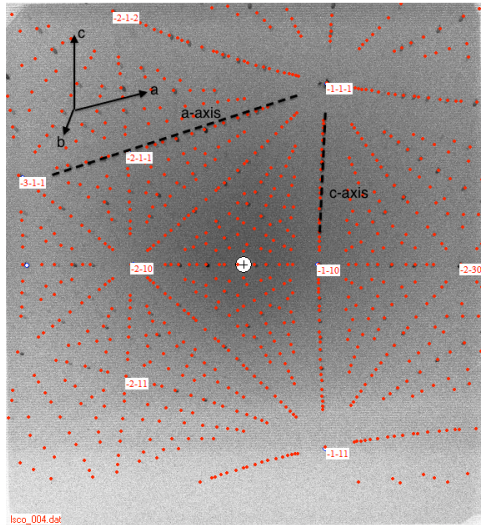


Figure 13: *Laue pictures of  $x = 0.04$  fitted by Orient Express. The red dots marks the Bragg peaks fitted over the black measured. Some selected Bragg peaks are labeled in relation to the  $[abc]$  plane. The black dotted lines show the  $a$ -axis and  $c$ -axis, and the orientation of the crystal is situated in the corner of the figure.*

### 6.3 Neutron Diffraction

The early Laue pictures taken at Risø showed promising signs of single crystal structure. While x-ray diffraction only measures the surface of the crystal, neutrons are able to measure the bulk of the crystal, which is why this is the next step in the analysis. In order to examine the bulk of the crystal, we used the Orion instrument at PSI<sup>10</sup>. One way to examine the structure is by looking at the specific planes inside the crystal. We wanted to look for the  $[004]$  plane and the  $[200]$  plane, which are highly reflective and therefore easier to detect and to obtain good results.

The experiment design followed two steps in general; another Laue alignment and the neutron scattering analysis. Firstly the crystals were fixed on a goniometer and the Laue method was again used to align the crystal. See the aligned Laue pictures and direction of crystal in appendix A.3. The pictures showed that the  $c$ -axis had not aligned along the longitudinal axis of the crystal. Furthermore the directions of the  $c$ -axis varied between the different crystals. With the orientation of the axes well known and marked, the sample was ready for testing.

Secondly the Orion instrument was used in the neutron scattering analysis. The Orion instrument is a two-axis diffractometer, with a wavelength of  $2.21 \text{ \AA}$ , usually used to align and check samples. In order to do so, the sample itself is situated on a mounting table. The sample can be rotated around three different axes, the rotation angles being denoted; phi ( $\phi$ ), chi ( $\chi$ ) and omega ( $\omega$ ), see illustration in figure 14.

The table was then placed between the beam outlet and the single He3-tube detector. See an illustration of the setup in figure 14. The detector was adjustable in such a way that the angle between the incident beam and detected scattered beam fulfills the Bragg conditions

<sup>10</sup>Paul Scherrer Institute (PSI), Switzerland.

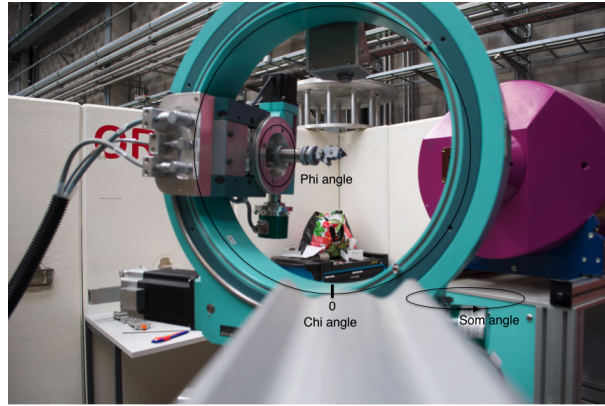


Figure 14: *Setup of Orion. In the picture the detector (purple) is shown along with the equipment controlling the chi angle (the turquoise circle). Attached in the center is the positioning table where the crystal is mounted. Omega (som) lies in the plane and when  $\chi = 0$ , omega and phi are coincident. This picture is taken from the position of the beam outlet.*

for the desired plane. The crystal on the table had to be positioned, such that the c-axis, when measuring the [004] plane, lay exactly in the vertical plane of the beam and detector. Furthermore the angle between the beam and the c-axis had to be exactly  $180-2\theta$  (the angle between the beam and the detector itself) if correct measurements of the [004] plane were to be done. The same applies for the a-axis when measuring the [200] plane. Measurements were then done by scanning the crystal within a given interval of degrees, both as an omega or chi scan.

The detector measures the intensity by counting the number of neutrons scattered by a certain angle. The intensity from a reflected Bragg peak is shown as a Gaussian shaped-like peak, measured as a function of the desired angle. Ideally, in a perfect single crystal and with a perfect beam, the peak would be a delta function, allowing scattering from the crystal only to be detected at one certain angle. The neutron beam has a natural divergence, which allows scattering to happen at more than one angle, and still be captured by the detector.

The amplitude of the intensity peak depends on the crystal plane and the mass of the crystal. A larger crystal will contain more unit cells than a smaller crystal, and therefore the amplitude of the intensity peak will be higher when measuring the same plane. However, it is only the part of the crystal that is hit by the neutron beam that contribute to the detected intensity. Furthermore, the cross section of the beam is not a perfect circle, this means that the orientation and positioning of the crystal has a significant influence on the measured intensity.

All in all, both the cross section of the neutron beam and the varying size of the crystals make it difficult to directly compare the amplitudes from the [004] plane in different crystals.

Figure 15 below shows three omega (som) scans of the [004] plane from  $x = 0.04$ ,  $x = 0.06$  and  $x = 0.07$ .

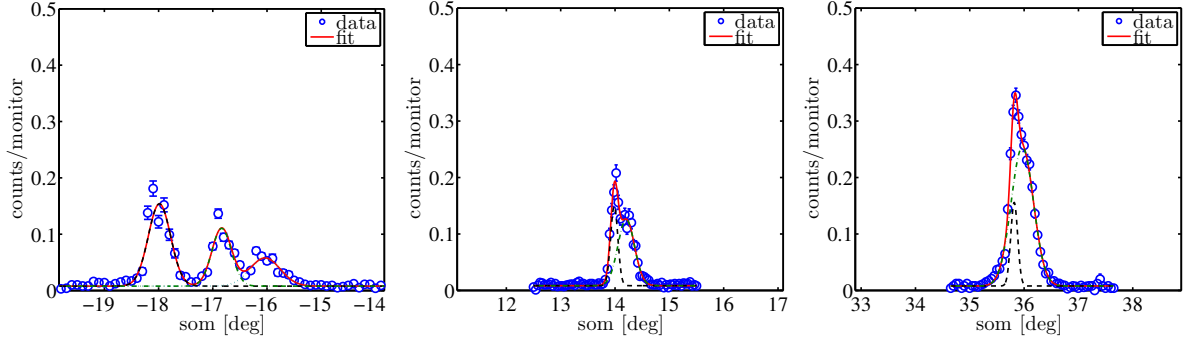


Figure 15: An omega scan of the intensity distribution within the (004) plane. From left to right:  $x = 0.04$ ,  $0.06$  and  $0.07$ . The blue dots shows the measured data along with the uncertainty, and the red line shows the fit. Notice the multiple peaks on both  $x = 0.04$  and  $0.06$ , indicating multiple crystals in  $x = 0.04$  and  $0.06$ .  $x = 0.07$  shows indication of being a single crystal. The background noise is due to incoherent scattering.

The figure to the left clearly shows three peaks. As stated earlier, a single crystal would only provide one intensity peak. What we see is a spread at the same value of  $2\theta$ . This means that all three peaks are the result of the [004] reflection. Several peaks at different rotations of the sample indicate multiple nonaligned domains within the crystal itself. These domains are often denoted as crystallites. This would result in multiple intensity peaks, as shown in the figure. With that in mind, the  $x = 0.04$  does not appear to be a single crystal.

The figure in middle shows one main peak with a smaller peak right next to it. The fact that the two peaks are that close together could be a sign of twinning. However, it is impossible to identify signs of twinning due to the fact that twinning appear on the a- and b-axes, and we are only measuring along the c-axis. Therefore is it likely to assume that we are instead looking at multiple nonaligned domains within the crystal itself, as it was the case in the previous figure.

The figure to the right shows one Gaussian peak without any secondary peaks. From this scan, it is likely to say that we are dealing with a single crystal.

From looking at these three omega scans of the [004] plane, it looks like  $x = 0.04$  is not a single crystal,  $x = 0.06$  is not a single crystal and  $x = 0.07$  is a single crystal. See omega scans from  $x = 0.05$  [004] and [200],  $x = 0.06$  [200] and  $x = 0.07$  [111] in appendix A.3. From the remaining scans it looks like  $x = 0.05$  is a single crystal from both the [004] and the [200] plane,  $x = 0.06$  is a single crystal and  $x = 0.07$  is not a single crystal.

A grid scan is a 2D intensity peak along two axes. It can provide more information than a 1D scan. An example of an omega/stt (position of the detector) scan can be seen in figure 26.

The interpretation of the grid scan is similar to the omega scans. If both the scans show only one peak, then it is a good indication that the structure is a single crystal. If on the other hand several peaks show at the same value of stt/ $2\theta$  but variable omega values, then it is an indication of multiple crystals with the same structure but aligned differently. If the scans show

a peaks at the same value of omega but variable  $stt/(2\theta)$  values then it is a sign of different crystals align with the same orientation, in other words; twinning.

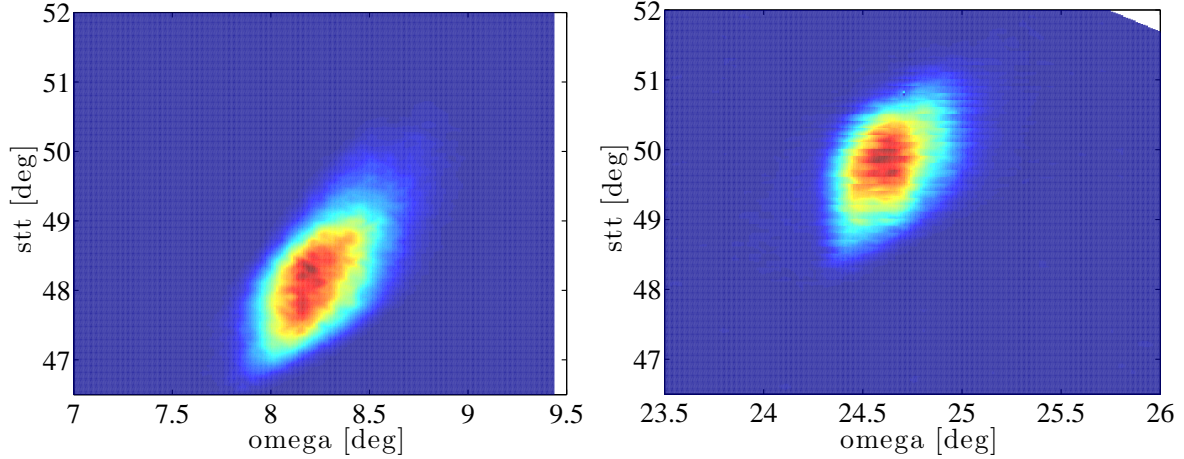


Figure 16: Grid scans of the  $x = 0.05$  crystal, showing the  $[200]$  and the  $[020]$  peak.

The figure above shows grid scans of the  $x = 0.05$  crystal of the  $[200]$  plane and the  $[020]$  plane. The intensity is at its highest in the red colored area and decreasing when going from red to blue. From the grid scans omega/ $stt$  it is possible to determine the lattice parameters of the crystal by using Bragg law. From Bragg law:  $d = n\lambda/2\sin\theta$ , where  $n = 2$  for  $[200]$  and  $[020]$ ,  $\lambda = 2.21 \text{ \AA}$  and  $2\theta \approx 49.82$  from the  $[200]$  peak and  $2\theta \approx 48.07$  from the  $[020]$  peak. From this the lattice parameters are estimated to be  $d_1 = 5.26 \text{ \AA}$  and  $d_2 = 5.44 \text{ \AA}$ , where  $a$  always denotes the lowest number so that  $a = 5.26 \text{ \AA}$  and  $b = 5.44 \text{ \AA}$ . These values vary quite a lot from what is expected (recall  $a \approx 5.36 \text{ \AA}$  and  $b \approx 5.41 \text{ \AA}$ ).

Grid scans from  $x = 0.05$  of the  $[004]$  plane and the  $[200]$  plane, scanning over  $h$  and  $l$ , and scans from  $x = 0.06$  of the  $[004]$  plane and the  $[200]$  plane, scanning over  $h$  and  $l$ , can be seen in appendix A.3. The scans show no signs of twinning or other impurities.

## 7 Discussion

### 7.1 Summary of Results

A brief summarization of the results from the data analysis:

**$x = 0.02$**  As a new method, the powder was mixed with ethanol. The powder showed promising signs in the FullProf analysis. Unfortunately a final crystal was never made, due to the fact that the powder was subjected to too much heat in the mirror furnace and a stable melting zone was not maintained for long enough. Even though the process was aborted prematurely, a small piece was still produced. Measurements were made using x-rays and the Laue pictures showed signs of twinning. No further measurements were made on the piece/crystal.

**$x = 0.03$**  A final crystal was produced but started to crumble within a few days. Measurements with x-rays were made on the crumbled crystal and an analysis in FullProf showed a

content of 54 mol% of  $\text{La}(\text{OH})_3$ . Due to an incomplete reaction,  $\text{La}_2\text{O}_3$  was left in the crystal.  $\text{H}_2\text{O}$  from the air had then reacted with the  $\text{La}_2\text{O}_3$ , which caused it to crumble. No further measurements were made.

**$x = 0.04$**  The Laue pictures taken at Risø were inconclusive, due to contradicting results. The fit from Orient Express indicated that the structure was very likely to be LSCO. The omega scan showed three peaks from the [004] plane and therefore it was most likely not a single crystal. The peak from the [200] plane was never found. A FullProf analysis of a  $x = 0.04$  solvent showed 78.10 mol% of CuO (intended was 80 mol%). The difference might be explained by the inaccuracy of the FullProf analysis. In conclusion  $x = 0.04$  is most likely not a single crystal.

**$x = 0.05$**  Several pictures were taken at Risø, each of these showed no sign of impurities. The structure was confirmed by Orient Express to be LSCO. Omega scans of the [004] plane and the [200] plane both showed a single peak. Grid scans of the [004] plane and the [200] plane measured along  $h$  and  $l$  showed no signs of twinning. Neither did the [200] plane and the [020] plane measured along omega and  $stt$ . In conclusion  $x = 0.05$  must be assumed to be a single crystal.

**$x = 0.06$**  The Laue pictures taken of  $x = 0.06$  showed signs of impurities and multiple peaks. However, the Laue alignment showed no significant irregularities. The omega scans showed multiple peaks from the [004] plane and a single peak from the [200] plane. The grid scans of the two planes did however show single spots with no signs of multiple peaks. In conclusion the results seems to be contradicting.  $x = 0.06$  most definitely consists of multiple peaks but may in some areas be a single crystal.

**$x = 0.07$**  The Laue alignment picture seems fine when looking along the  $c$ -axis, but along the  $a$ -axis the spots look a bit blurry. The FullProf analysis of the unheated powder showed a content of 7.09 mol% of unreacted  $\text{La}_2\text{O}_3$ , the reason for this has not been found. Additional CuO was added to the powder before the compression phase. Orient Express confirmed the structure to be LSCO, and omega scans from the [004] plane and the [111] plane both showed single peaks, indicating that  $x = 0.07$  is a single crystal.

## 7.2 Discussion of Results

Growing single crystals has been a slow and challenging process. Many attempts have failed, which is why a final product of four, more or less single, crystals is a great achievement. A lot of things can go wrong, and in the following I will comment on some of the pitfalls, and explain how the process could be optimized.

First up is the making of a proper powder. It is important to ensure a complete reaction without any unreacted  $\text{La}_2\text{O}_3$ . One experiment, where ethanol was used to create a 'mixing effect', showed good results. However, more experiments have to be conducted specifically to determine whether the ethanol-based method is better than the shaker method.

The FullProf analysis of  $x = 0.07$  powder showed signs of unreacted  $\text{La}_2\text{O}_3$ . Afterwards was additional CuO added to the powder. A later analysis showed signs of a single crystal structure, and therefore it must be presumed that the unreacted  $\text{La}_2\text{O}_3$  had reacted with the added CuO.

A second key element is the compression phase. In this phase it is crucial that the compressed powder is turned in to a completely straight rod. If the rod is not completely straight the heat

from the furnace will not be evenly distributed. Optimizing this phase is at present time limited by the equipment used.

The last, and most challenging part of the process, is the mirror furnace. A lot of adjustable parameters, such a temperature, melting rate etc., makes this process the most vulnerable. For one, the molten zone is extremely fragile, and subjecting the solvent to too much heat in the beginning will ruin the rest of the process – as it was the case of  $x = 0.02$ . In order to avoid similar incidents it is vital to subject the solvent to an appropriate amount of heat. Secondly, to be able to sustain the molten zone, the grow rate needs to be constant. This will prevent too much of the CuO to evaporate. The extra added 3 mol% CuO seemed to work as intended in order to maintain a stable molten zone. But even though a crystal was grown using this method, it could be interesting to use oxygen pressure instead, as described in section 5.2.3. Thirdly, experience shows that if a steady state is not found within the first few hours the solidified crystal will not be single crystal.

All in all, an optimized and standardized process needs to be developed in order to ensure a more effective crystal-growing process.

In order to determine why some crystals turned out fine while others did not, we have to look at each crystal individually. Unfortunately we do not have cohesive measurements of all crystals, which makes it difficult to identify where any potential errors were made. Due to a lack of measurements it is not possible to determine whether the fault lies in the production of the powder or in furnace process. By looking at the grow sheets from the mirror furnace process it has not been possible to determine why some crystals turned out better than others. The exception being  $x = 0.02$  as previously mentioned. Ideally x-ray measurements of all of the powders should have been made, as well as neutron scattering experiments on all of the crystals. In this way consistent and organized data would have been at hand, making the process of troubleshooting a lot easier.

### 7.3 Outlook

This thesis concerns how to grow a single crystal, and the experimental analysis required to determine the quality and outcome of the growing process. However, these are only the preliminary measurements, and much more information is to be extracted about the crystals. First is to measure the susceptibility and electrical resistivity of the crystal. Secondly, the orthorhombicity as a function of the temperature needs to be measured in order to discover the position of the phase transition from tetragonal to orthorhombic structure. This is done by measuring at what time the [014] peak disappears. Last up is to look at whether the crystal has an incommensurable (IC) magnetic order with and without an external magnetic field, and perhaps even to look at whether (IC) fluctuations might occur. Finally the crystals will be sent to the U.S. to be super-oxidized to  $\text{La}_{2-x}\text{Sr}_x\text{CuO}_{4+\delta}$  and all of the above measurements are to be repeated with the resulting new doping.

## 8 Conclusion

We were able to grow LSCO crystals with different Sr doping. The following amounts of doping was used:  $x = 0.02, 0.03, 0.04, 0.05, 0.06$  and  $0.07$ . From analyzing the measurements made

using neutron scattering it can be concluded that  $x = 0.04$  is not a single crystal,  $x = 0.05$  is a single crystal,  $x = 0.06$  is properly a single crystal and  $x = 0.07$  probably a single crystal.  $x = 0.02$  was subject to too much heat, which ruined the sample. However, the experiment of mixing the powder with ethanol showed promising results, but further testing needs to be done.  $x = 0.03$  had a high content of unreacted  $\text{La}_2\text{O}_3$  which caused the sample to crumble.

All in all it can be concluded that the method used is capable of creating single crystals. It has become clear that the process is very fragile, and a lot of parameters have to be taken into account in order to ensure a good result. Special attention needs to be paid while growing the crystal in the mirror furnace, since the crystals are highly sensitive to heat. The 3 mol% added CuO worked as a suitable replacement of a pressured oxygen atmosphere in creating a stable molten zone. However, the method needs to be optimized and automatized in order to be able to efficiently and consistently grow single crystals.

## References

- [1] J.F. Annett, *Superconductivity, Superfluids and Condensates*, Oxford University Press Inc., New York (May 2003)
- [2] A.C. Rose and E.H. Rhoderick, *Introduction to Superconductivity*, University of Manchester Institute of Science and Technology, U.K. (10. jun. 1976)
- [3] L. Udby *et al.*, Phys. Rev. B. **80** 014505 (2009)
- [4] Kim Lefmann, *Magnetic Neutron Scattering notes*, Niels Bohr Institute (2011)
- [5] C. Kittel, *Introduction to Solid State Physics - EIGHTH EDITION*, 8th ed, Jon Wiley and Sons (2005)
- [6] S. Blundell, *Magnetism in Condensed Matter*, University of Oxford, New York (2007)
- [7] K. Oka and H. Unoki *Japanese Journal of Applied Physics, vol 26 L1590* (1987)
- [8] M. Napoletano and J.M. Gallardo Amores, *Journal of Crystal Growth* 712, (1989)
- [9] M. Napoletano and J.M. Gallardo Amores, *Physica C* 319 229, (1999)
- [10] J. Rodriguez-Carvajal, *Physica B* 192 55, (1993)
- [11] A. T. Rømer *Master Thesis*, Niels Bohr Institute (August 2009)
- [12] T. Schneider and J.M. Singer, *Phase Transition Approach to High Temperature Superconductivity*, University of Zurich, Switzerland
- [13] C. Michel and D. Pavuna, *Introduction to Superconductivity and High- $T_c$  Materials*, World Scientific Publishing (1992)
- [14] Orient Express,  
from Webpage:  
<http://www.ill.eu/instruments-support/computing-for-science/cs-software/all-software/orientexpress/>, Web. 09 June 2014.
- [15] Figure 3: Cooper Pairs,  
from Webpage: <http://hyperphysics.phy-astr.gsu.edu/hbase/solids/coop.html>, Web. 09 June 2014.
- [16] Figure 5: LSCO Structure,  
from Webpage: <https://staff.aist.go.jp/h-eisaki/LSCO.html>, Web. 09 June 2014.
- [17] Figure 6: Phase Diagram,  
from Webpage: [http://www.spring8.or.jp/en/news\\_publications/press\\_release/2011/110429/](http://www.spring8.or.jp/en/news_publications/press_release/2011/110429/),  
Web. 09 June 2014.
- [18] Figure 7: Bragg Law,  
from Webpage: <http://www.globalsino.com/EM/page3882.html>, Web. 10 June 2014.

## A Appendix

### A.1 Example of a 100 g batch with doping $x = 0.02$

Table 1: Table of Values

Compound	Copper	Strontium	Lanthanum	Oxygen
Chemical formula	Cu	Sr	La	O
Molar mass $M$ [g/mol]	63.546	87.62	138.905	15.999
Compound	Copper (II) oxide	Strontium carbonate	Lanthanum (II) oxide	
Chemical formula	CuO	SrCO <sub>3</sub>	La <sub>2</sub> O <sub>3</sub>	
Molar mass $M$ [g/mol]	79.545	147.63	325.809	

Molar mass of La<sub>1.98</sub>Sr<sub>0.02</sub>CuO<sub>4</sub>:

$$M_{\text{LSCO } 2\%} = 1.98M_{\text{La}} + 0.02M_{\text{Sr}} + 1.03M_{\text{Cu}} + 4M_{\text{O}} = 406.233 \text{ g/mol}$$

The 100 g of mixed compound hence is the following number of moles:

$$n_{\text{LSCO } 2\%} = m_{\text{total}}/M_{\text{LSCO } 2\%} = 0.2462 \text{ mol}$$

The following amount of each powder is needed:

$$\begin{aligned} m_{\text{CuO}} &= 1.03 n_{\text{LSCO } 2\%} \times M_{\text{CuO}} = 20.1686 \text{ g} \\ m_{\text{SrCO}_3} &= 0.02 n_{\text{LSCO } 2\%} \times M_{\text{SrCO}_3} = 0.7268 \text{ g} \\ m_{\text{La}_2\text{O}_3} &= 1.98/2 n_{\text{LSCO } 2\%} \times M_{\text{La}_2\text{O}_3} = 79.4005 \text{ g} \end{aligned}$$

### A.2 Example of a 10 g batch for solvents with doping $x = 0.02$

The following amount of each powder is needed:

$$\begin{aligned} n_{\text{CuO}} &= 0.8 \Rightarrow m_{\text{CuO}} = n_{\text{CuO}} \times M_{\text{CuO}} = 63.6360 \text{ g} \\ n_{\text{SrCO}_3} &= 0.2 \times 0.02 \Rightarrow m_{\text{SrCO}_3} = n_{\text{SrCO}_3} \times M_{\text{SrCO}_3} = 0.5905 \text{ g} \\ n_{\text{La}_2\text{O}_3} &= 0.2 \times (1 - 0.02/2) \Rightarrow m_{\text{La}_2\text{O}_3} = n_{\text{La}_2\text{O}_3} \times M_{\text{La}_2\text{O}_3} = 64.5102 \text{ g} \end{aligned}$$

This gives  $m_{\text{total}} = 128.7367 \text{ g}$ . For a batch of 10 g the following amounts are needed: 4.9431 g of CuO, 0.04587 g of SrCO<sub>3</sub> and 5.0110 g of La<sub>2</sub>O<sub>3</sub>.

### A.3 Figures from the data analysis

#### A.3.1 Orient Express

$x = 0.05$

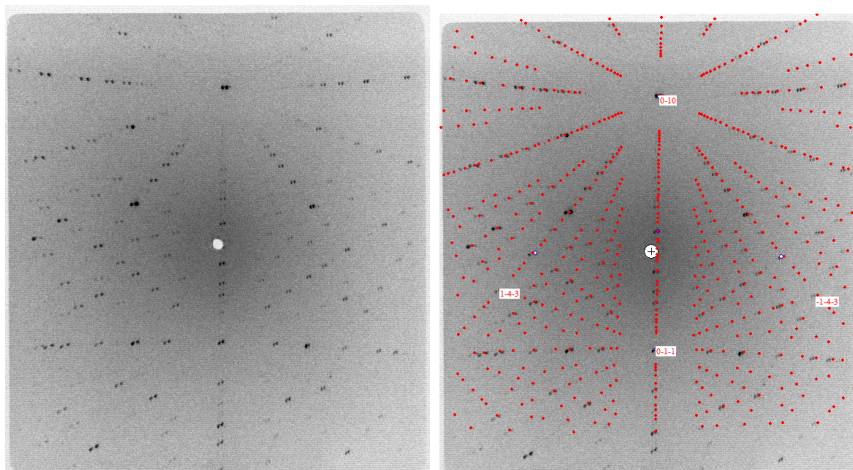


Figure 17: Laue picture of  $x = 0.05$ . (Left) the original laue picture and (right) fit from Orient Express. The red dots marks the Bragg peaks fitted over the black measured.

$x = 0.07$

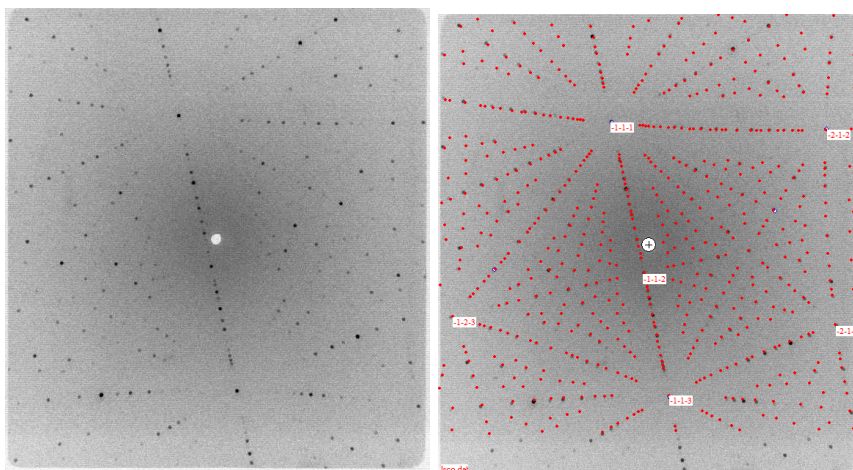


Figure 18: Laue picture of  $x = 0.07$ . (Left) the original laue picture and (right) fit from Orient Express. The red dots marks the Bragg peaks fitted over the black measured.

### A.3.2 Crystal Alignment

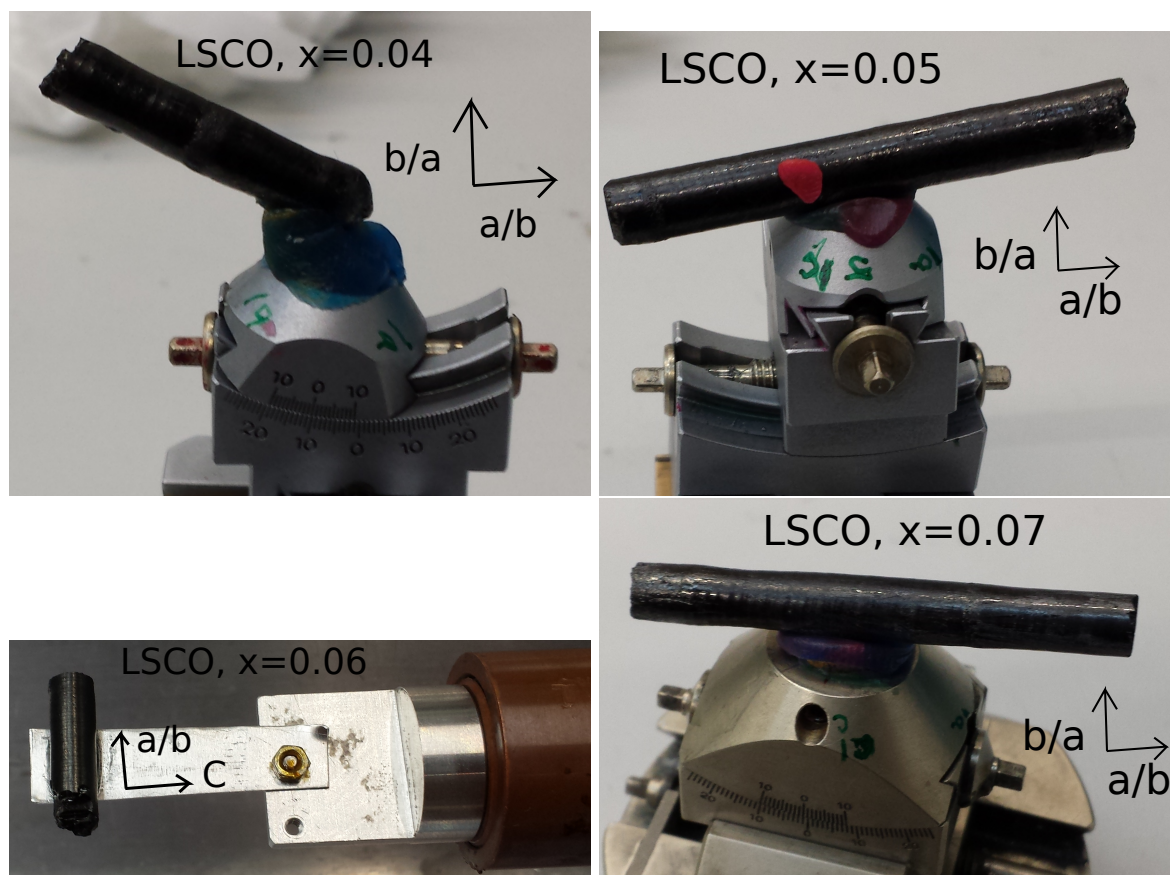


Figure 19: Pictures of the samples with the crystal axes marked. We could not distinguish between the  $a$  and  $b$  axes in this experiment.

### Masses

Crystal	Mass(g)
0.02	0.6495
0.04	4.2700
0.05	8.3432
0.06	2.3328
0.07	9.2322

Table 2: Mass of the crystals.

### A.3.3 $x = 0.04$

#### Laue Pictures

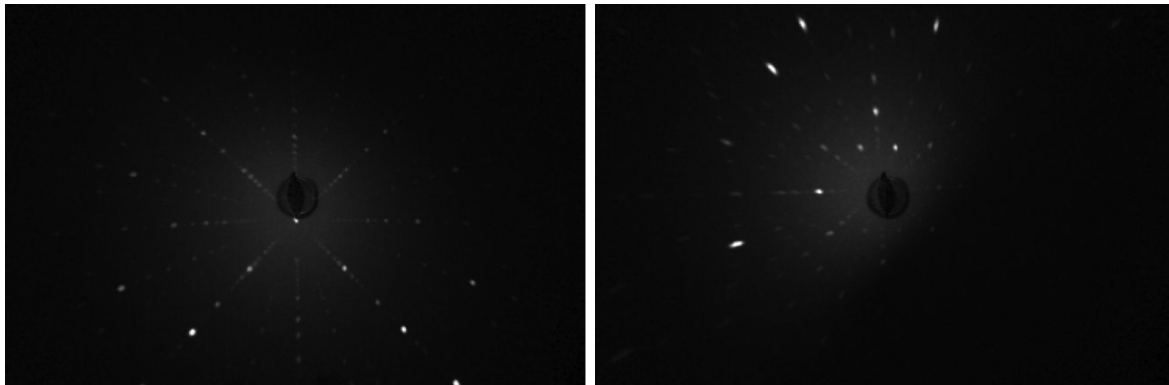


Figure 20: *Laue picture of the upper part of the  $x = 0.04$  crystal, with the  $c$  (left) and  $a$  (right) axis pointing along the beam.*

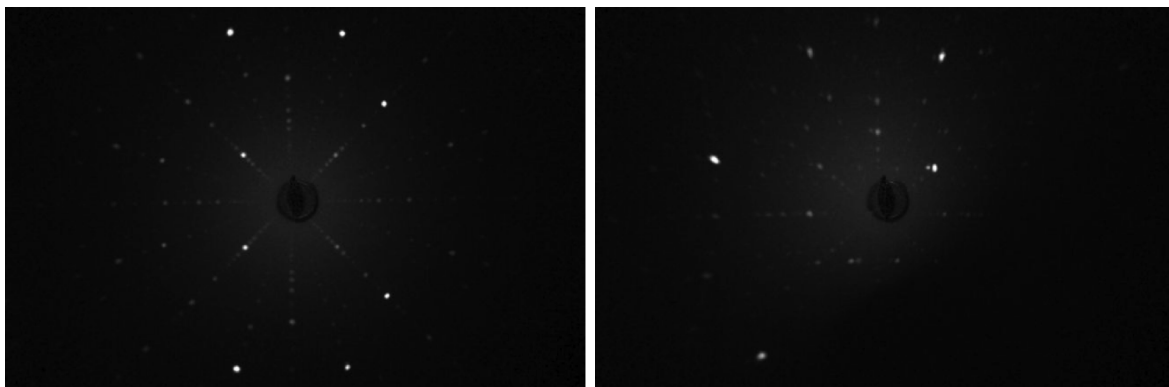


Figure 21: *Laue picture of the lower part of the  $x = 0.04$  crystal, with the  $c$  (left) and  $a$  (right) axis pointing along the beam.*

## Omega Scans

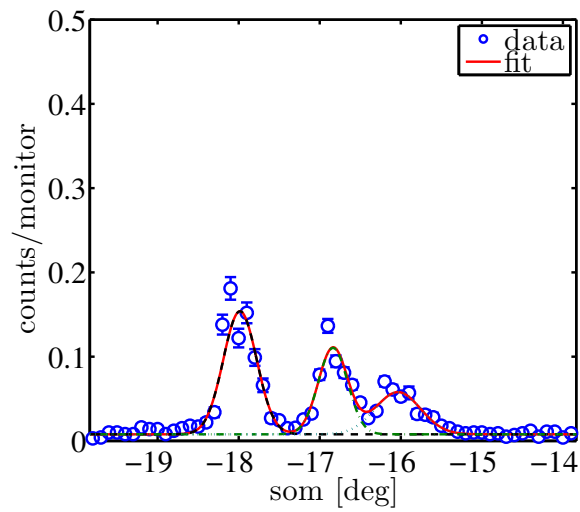


Figure 22: The  $[004]$  peak of the  $x = 0.04$  crystal, measured at Orion. We see that the crystal is not a single crystal. The  $[200]$  peak was not measured.

### A.3.4 $x = 0.05$

#### Laue Pictures

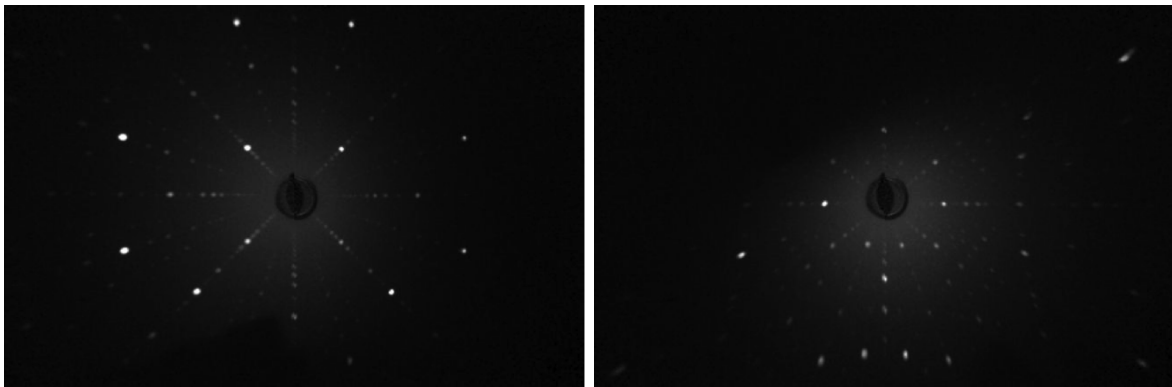


Figure 23: Laue picture of the  $x = 0.05$  crystal, with the  $c$  (left) and  $a$  (right) axis pointing along the beam.

### Omega scans

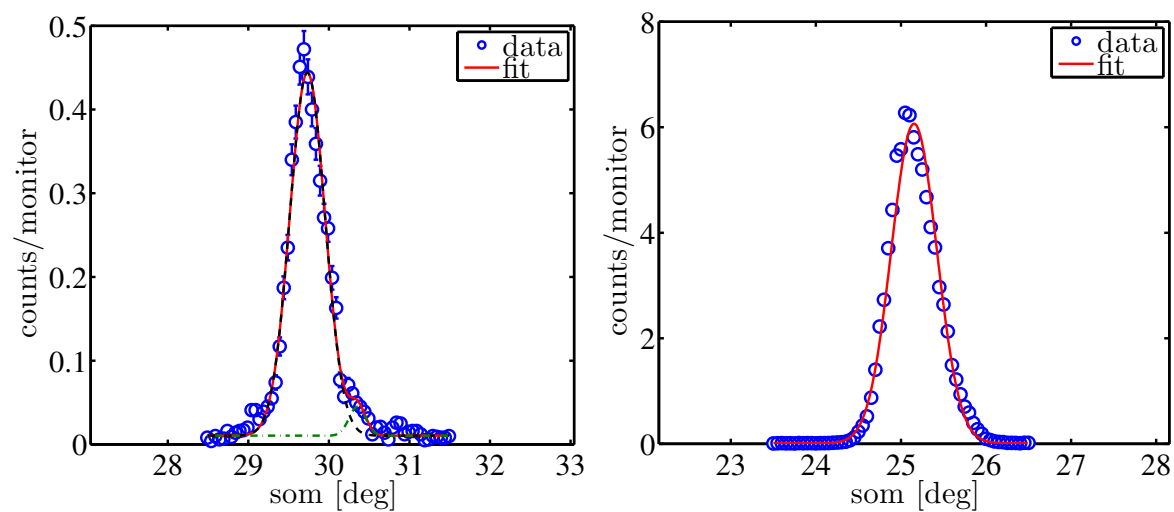


Figure 24: The  $[004]$  (left) and the  $[200]$  (right) peaks of the  $x = 0.05$  crystal, measured at Orion.

### Grid scans

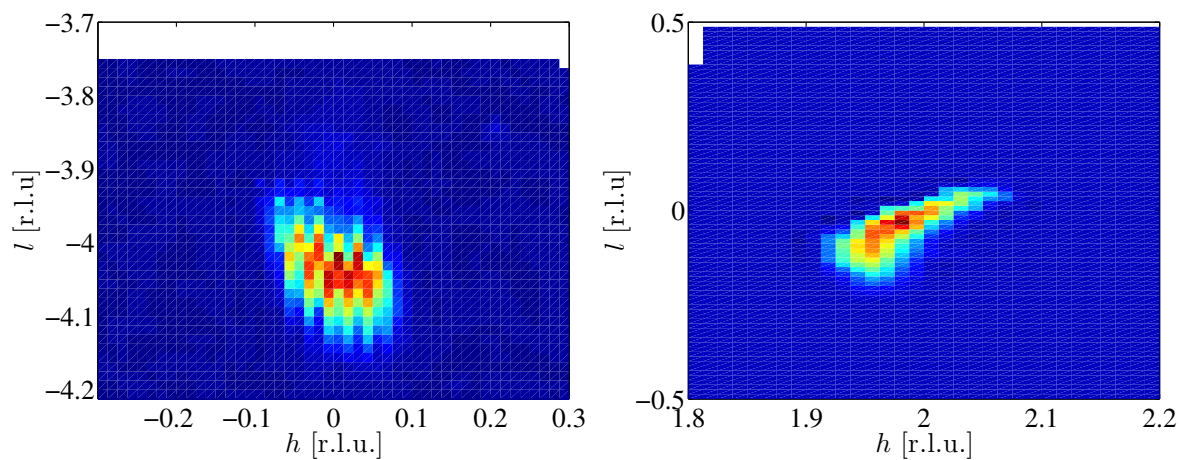


Figure 25: Grid scans of the  $x = 0.05$  crystal, showing the  $[004]$  and the  $[200]$  peak.

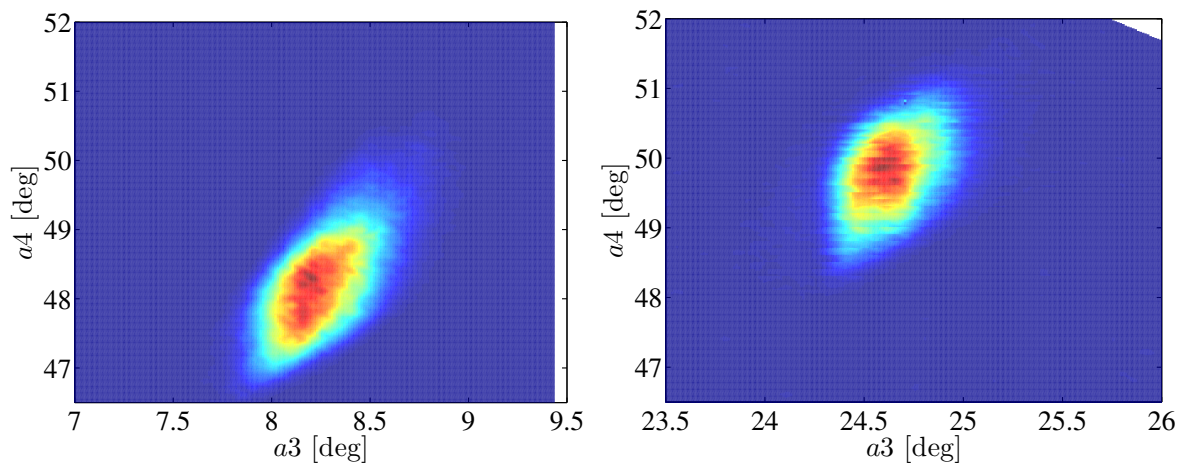


Figure 26: Grid scans of the  $x = 0.05$  crystal, showing the  $[200]$  and the  $[020]$  peak. The positions of  $a4$  can be used to determine the lattice parameters.

### A.3.5 $x = 0.06$

#### Laue Pictures

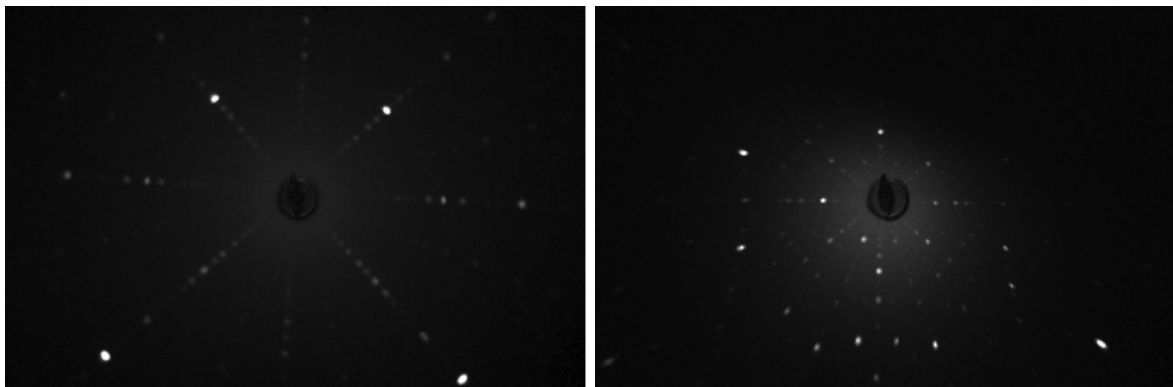


Figure 27: Laue picture of the  $x = 0.06$  crystal, with the  $c$  (left) and  $a$  (right) axis pointing along the beam.

## Omega scans

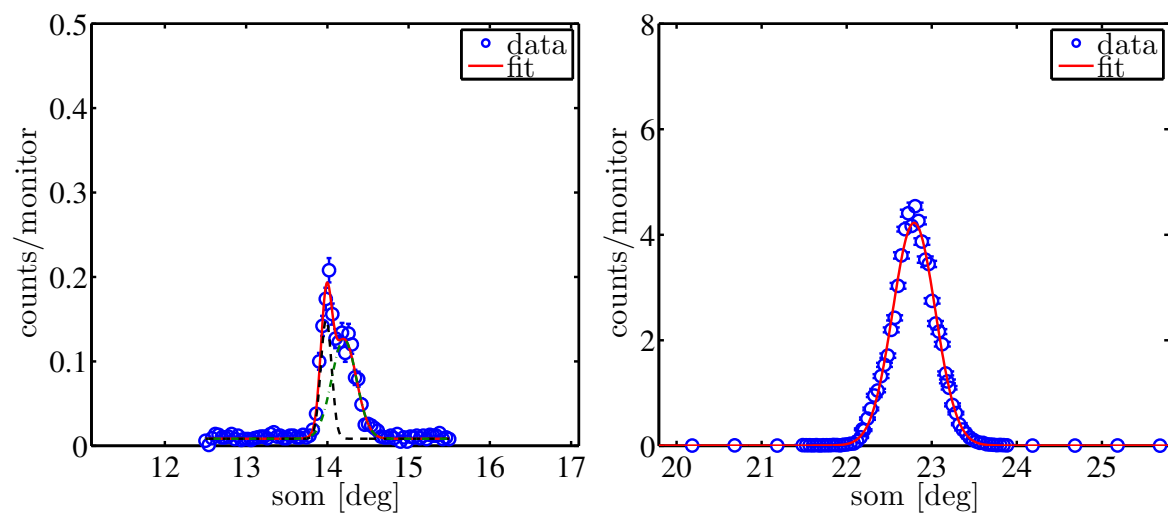


Figure 28: The  $[004]$  (left) and the  $[200]$  (right) peaks of the  $x = 0.06$  crystal, measured at Orion. The  $[004]$  peak shows twinning.

## Grid scans

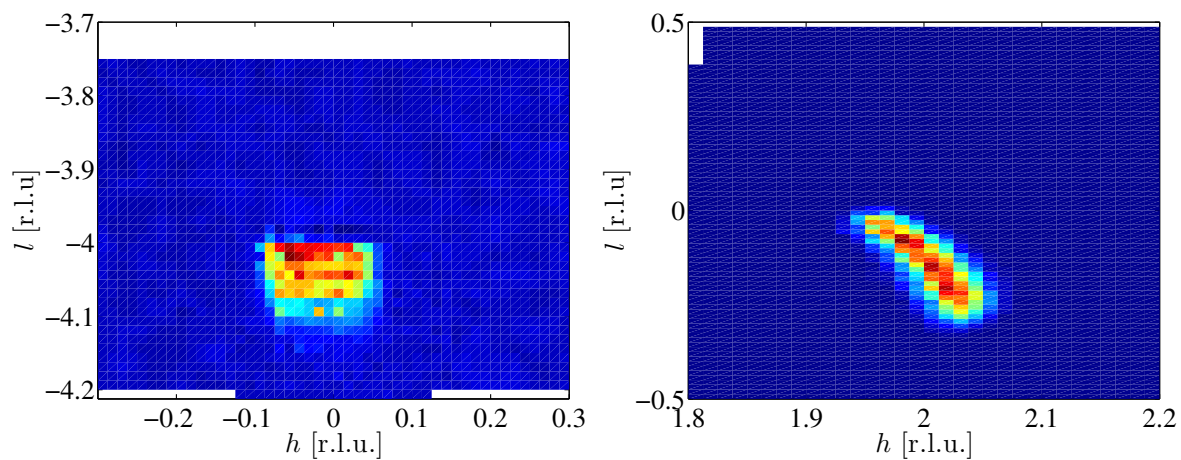


Figure 29: Grid scans of the  $x = 0.06$  crystal, showing the  $[004]$  and the  $[200]$  peak.

### A.3.6 $x = 0.07$

#### Laue Pictures

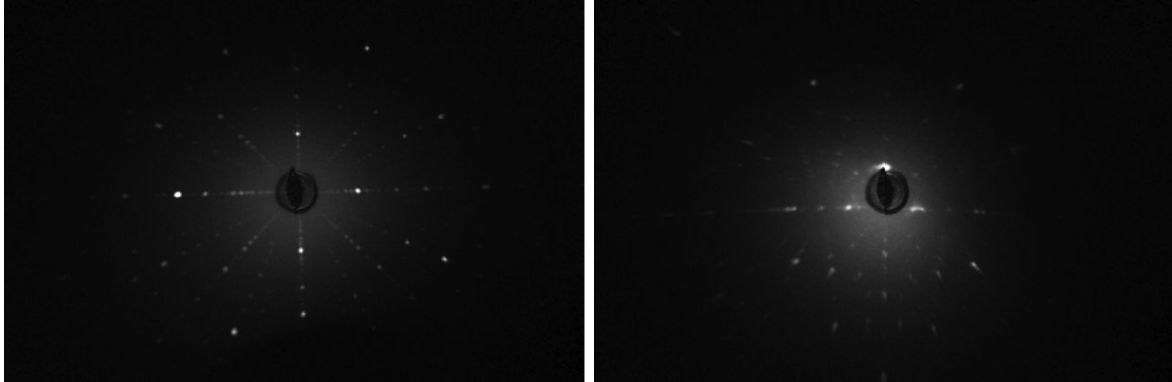


Figure 30: Laue picture of the  $x = 0.07$  crystal, with the  $c$  (left) and  $[110]$  (right) axis pointing along the beam.

#### Omega scans

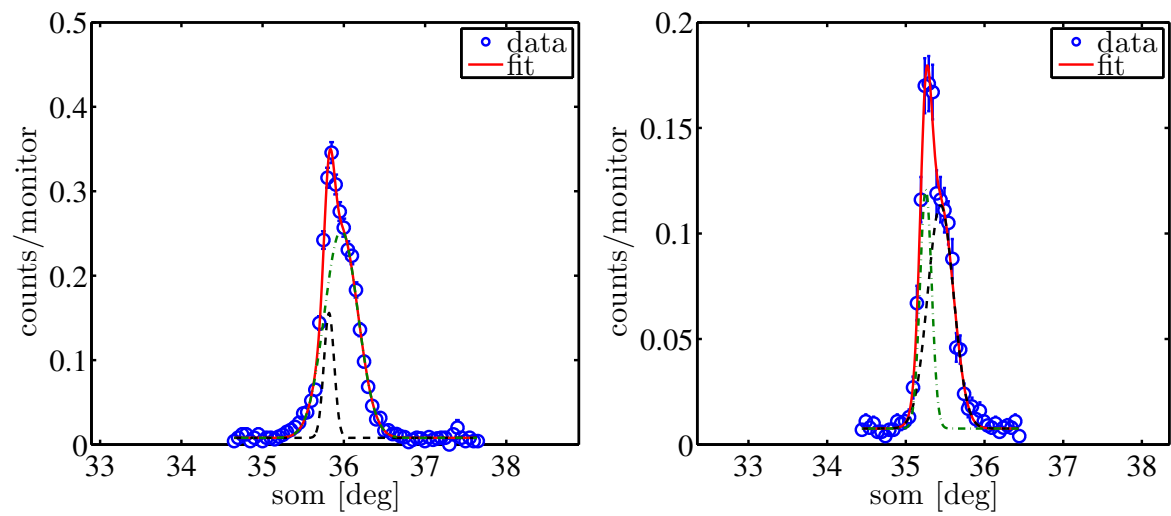


Figure 31: The  $[004]$  (left) and the  $[111]$  (right) peaks of the  $x = 0.07$  crystal, measured at Orion. The  $[111]$  was measured because the crystal was accidentally rotated by 45 degrees in the Laue, and thus we had difficulties finding the  $a$  and  $b$  axes.

### A.3.7 Overview

#### [004] Omega Scans

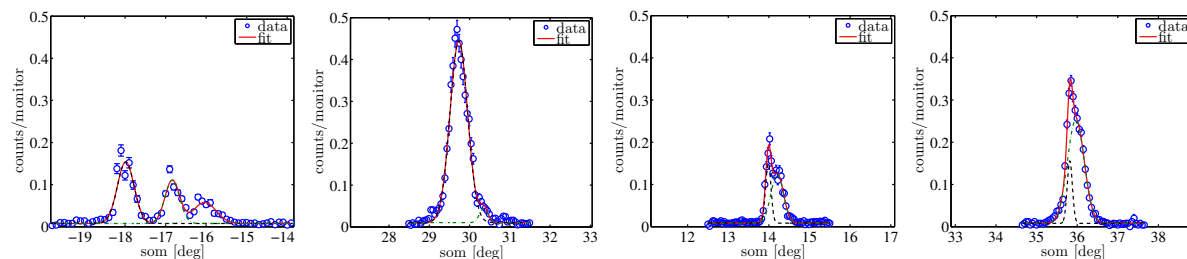


Figure 32: The [004] peak for all the samples, from left to right:  $x = 0.04$ ,  $0.05$ ,  $0.06$  and  $0.07$ .

#### [200] Omega Scans

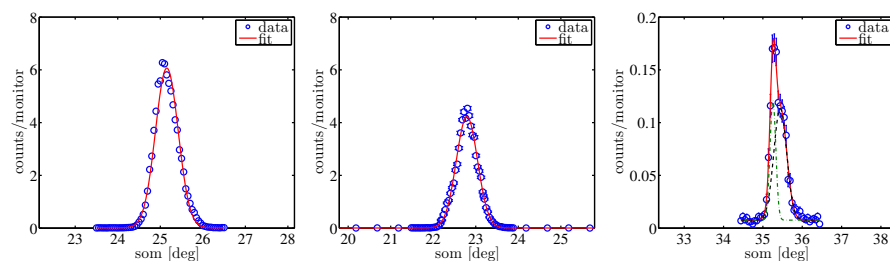


Figure 33: The [200] peak for the  $x = 0.05$  and the  $x = 0.06$  samples, from left to right. The rightmost is the [111] peak for the  $x = 0.07$  sample.

